A preoptic neuronal population controls fever and appetite during sickness

https://doi.org/10.1038/s41586-022-04793-z

Received: 17 February 2020

Accepted: 21 April 2022

Published online: 08 June 2022

Check for updates

Jessica A. Osterhout[1,2], Vikrant Kapoor[1,2], Stephen W. Eichhorn[2,3,4], Eric Vaughn[1,2], Jeffrey D. Moore[1,2], Ding Liu[1,2], Dean Lee[1,2], Laura A. DeNardo[5,6], Liqun Luo[5], Xiaowei Zhuang[2,3,4] & Catherine Dulac[1,2]✉

During infection, animals exhibit adaptive changes in physiology and behaviour aimed at increasing survival. Although many causes of infection exist, they trigger similar stereotyped symptoms such as fever, warmth-seeking, loss of appetite and fatigue[1,2]. Yet exactly how the nervous system alters body temperature and triggers sickness behaviours to coordinate responses to infection remains unknown. Here we identify a previously uncharacterized population of neurons in the ventral medial preoptic area (VMPO) of the hypothalamus that are activated after sickness induced by lipopolysaccharide (LPS) or polyinosinic:polycytidylic acid. These neurons are crucial for generating a fever response and other sickness symptoms such as warmth-seeking and loss of appetite. Single-nucleus RNA-sequencing and multiplexed error-robust fluorescence in situ hybridization uncovered the identity and distribution of LPS-activated VMPO ($VMPO^{LPS}$) neurons and non-neuronal cells. Gene expression and electrophysiological measurements implicate a paracrine mechanism in which the release of immune signals by non-neuronal cells during infection activates nearby $VMPO^{LPS}$ neurons. Finally, we show that $VMPO^{LPS}$ neurons exert a broad influence on the activity of brain areas associated with behavioural and homeostatic functions and are synaptically and functionally connected to circuit nodes controlling body temperature and appetite. Together, these results uncover $VMPO^{LPS}$ neurons as a control hub that integrates immune signals to orchestrate multiple sickness symptoms in response to infection.

During infection, the brain orchestrates evolutionarily conserved behavioural and physiological symptoms aimed at eliminating pathogens and increasing survival. Symptoms include fever, lethargy, appetite loss, warmth-seeking, social withdrawal and increased pain sensitivity[1]. Fever, a key symptom of infection, is elicited by pathogen-associated molecules that trigger the release of pro-inflammatory signals by immune cells[2,3]. These secreted signals interact with brain endothelial cells in circumventricular organs, where the blood–brain barrier is permeable, which enables the further production and propagation of immune signals within the brain[4]. One such circumventricular organ, the vascular organ of lamina terminalis (OVLT), is located in the preoptic area of the hypothalamus, where major homeostatic functions such as body temperature, thirst and sleep are regulated[5]. Specifically, thermoregulatory neurons in the preoptic area regulate body temperature by sensing ambient warmth and activating autonomic and behavioural circuits to decrease body temperature[6–8]. The preoptic area is also crucial for fever generation[9,10], and loss of the pro-inflammatory prostaglandin E_2 (PGE_2) receptor EP_3 in this region leads to a reduced febrile response[11,12]. However, which cell populations are responsible for generating fever, how they modulate circuits controlling body temperature and whether they affect other sickness symptoms are unknown. Here we sought to identify fever-generating neurons and determine their influence on sickness behaviours to provide new insights into the mechanisms by which the brain responds to infection.

Brain areas activated during fever

To generate fever, we injected the pro-inflammatory agents LPS or polyinosinic:polycytidylic acid (poly(I:C)), which mimic bacterial or viral infection, respectively, into mice. Body temperature peaked 2 h following LPS and poly(I:C) administration, with similar magnitudes and time scales (Fig. 1a, b and Extended Data Fig. 1a). LPS was therefore used in all subsequent experiments. Twelve brain areas showed a significant increase in Fos^+ cells following LPS administration, including regions involved in appetite, metabolism, thermoregulation, sleep, stress and fear responses (Fig. 1a, c and Extended Data Fig. 1b,c). Notably, cells within the VMPO (Fig. 1d–f, arrowheads) and lining the adjacent ventricle (Fig. 1d–f, arrow) were highly activated compared with controls. Activated VMPO neurons were inhibitory (mean ± s.e.m. was 88 ± 1% $VGAT^+$ and 6.8 ± 1.4% $VGLUT2^+$; Extended Data Fig. 1d, e) and distinct from previously described warm-sensitive neurons located more anterior–dorsal in the anteroventral periventricular nucleus (AVPe) and the

[1]Department of Molecular and Cellular Biology, Howard Hughes Medical Institute, Harvard University, Cambridge, MA, USA. [2]Center for Brain Science, Harvard University, Cambridge, MA, USA. [3]Department of Chemistry and Chemical Biology, Howard Hughes Medical Institute, Harvard University, Cambridge, MA, USA. [4]Department of Physics, Howard Hughes Medical Institute, Harvard University, Cambridge, MA, USA. [5]Department of Biology, Howard Hughes Medical Institute, Stanford University, Stanford, CA, USA. [6]Present address: Department of Physiology, University of California Los Angeles, Los Angeles, CA, USA. ✉e-mail: dulac@fas.harvard.edu

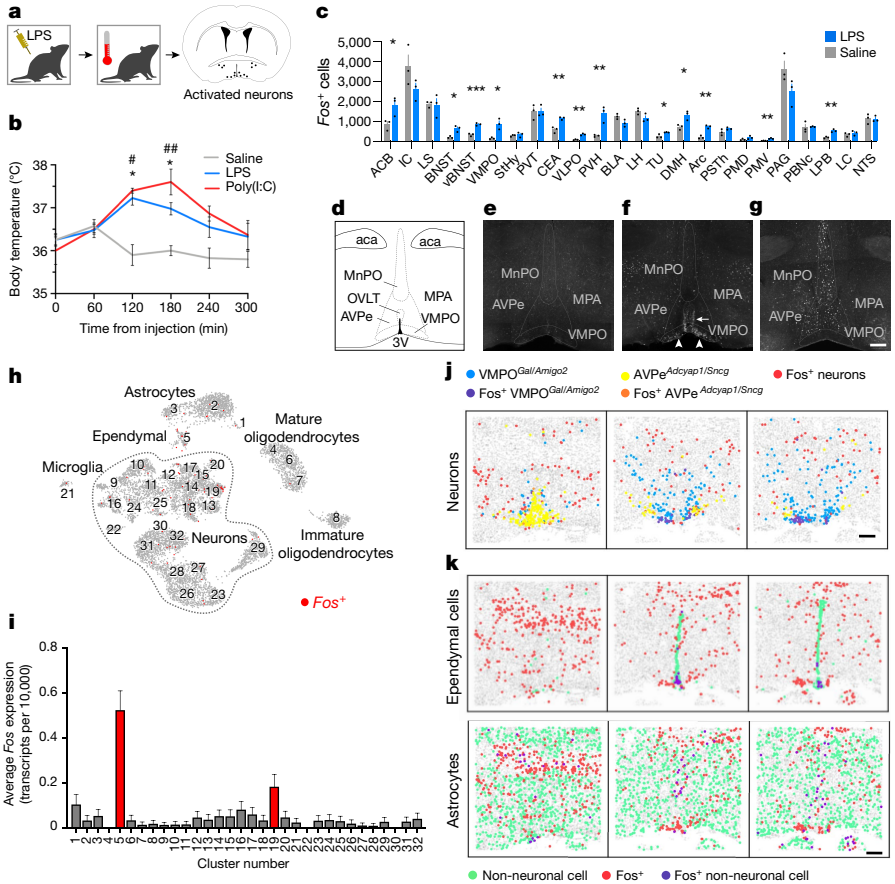

Fig. 1 | Activation of a specific VMPO neuronal population after LPS administration. a, Schematic of the experiment. Mice given an intraperitoneal injection of LPS or poly(I:C) were monitored for changes in body temperature and brain *Fos* expression. **b**, Mean body temperature following injection of saline, LPS or poly(I:C), two-tailed *t*-test, saline vs. LPS indicated by asterisks, $^{*}P < 0.05$, saline vs. poly(I:C) indicated by hash symbols $^{\#}P < 0.05$, $^{\#\#}P < 0.01$. Time zero is before injection. $n = 10$ per group. **c**, Mean number of Fos^{+} cells per brain nucleus. $n = 3$ per group, two-way analysis of variance (ANOVA), for all graphs. $^{*}P < 0.05$, $^{**}P < 0.01$, $^{***}P < 0.001$. **d**, Nuclei within the anterior preoptic region (see Extended Data Table 3 for definitions of brain area abbreviations). **e**–**g**, Fos expression after injection of saline (**e**), LPS (**f**) or warm-temperature challenge (**g**). Arrowheads indicate LPS-activated cells in the VMPO, and arrows indicate LPS-activated cells lining the ventricle. **h**, Uniform manifold approximation and projection representation of 32 cell clusters identified by snRNA-seq. **i**, Mean expression of *Fos* in snRNA-seq clusters (16,430 total nuclei, 5 pooled mice). Red bars indicate statistical significance, two-sided Mann–Whitney test ($P < 0.05$). **j**, Representative spatial distribution of selected cell populations identified by MERFISH at approximately bregma +0.2 mm, +0.0 mm and −0.2 mm. **k**, Representative spatial distribution of ependymal cells (top) and astrocytes (bottom) identified by MERFISH in the preoptic region. All error bars represent the s.e.m. Scale bar, 200 µm (**e**, **j** and **k**).

median preoptic nucleus (MnPO)[6] (Fig. 1g). On the basis of their proximity to the OVLT circumventricular organ[9], we hypothesized that $VMPO^{LPS}$ cells may represent the long sought-after fever-generating neurons.

Characterization of $VMPO^{LPS}$ neurons

To characterize $VMPO^{LPS}$ cells, we used a combination of single nuclear RNA-sequencing (snRNA-seq) and multiplexed error-robust fluorescence in situ hybridization (MERFISH)[13,14]. snRNA-seq data from 16,430 nuclei from VMPO cells from mice injected with saline or LPS, integrating both conditions[15], identified 32 neuronal and non-neuronal clusters (Fig. 1h). *Fos* expression was uniformly low in controls, which enabled us to examine LPS-treated samples for average *Fos* expression levels and the fraction of Fos^{+} cells within each cluster. Neuronal cluster 19 (characterized by *Galanin*, *Calcr* and *Amigo2* expression) and non-neuronal cluster 5 exhibited significant *Fos* enrichment (Fig. 1h, i and Extended Data Fig. 1f, g). Similarly, MERFISH analysis of LPS-treated mice identified a VMPO neuronal cluster previously named I-7 (ref. [13]) (here referred to as $VMPO^{Gal/Amigo2}$) that was characterized by the same genetic markers as snRNA-seq cluster 19 and displayed the highest fraction of Fos^{+} neurons[13] (Fig. 1j and Extended Data Fig. 1h). By contrast, warm-sensitive neurons, identified as cluster E-3 or $AVPe^{Adcyap1/Sncg}$ were only weakly activated by LPS (Fig. 1j and Extended Data Fig. 1h). Accordingly, in situ expression of LPS-induced *Fos* displayed high overlap with *Galanin*, *Calcr* and *Amigo2*, but not with *Adcyap1* (Extended Data Fig. 1i, j).

Endothelial and ependymal cells at circumventricular organs are involved in the signalling, production and translocation of pyrogenic cytokines and prostaglandins from the periphery to the brain[4,16,17], with local astrocytes and microglia producing additional immune signals[1,2]. LPS-activated snRNA-seq cluster 5 expressed markers for ependymal cells (*Lrp2* and *Aqp4*)[13,18] and activated astrocytes (*Gfap*)[19] (Fig. 1i and Extended Data Fig. 1g). Similarly, MERFISH identified astrocytes, endothelial cells, ependymal cells and mature oligodendrocytes as significantly enriched in *Fos* expression (Extended Data Fig. 2b). This activation appeared to be specific to LPS-induced responses, as there was no significant *Fos* enrichment in non-neuronal cells after aggression, mating or parenting episodes (Extended Data Fig. 2b).

We next investigated how $VMPO^{LPS}$ neurons are activated. Notably, within the $VMPO^{Gal/Amigo2}$ cluster, approximately 90% of Fos^{+} neurons were localized within 200 µm from the base of the brain, near the OVLT (Fig. 1j and Extended Data Fig. 2a). Moreover, strong *Fos* expression was seen in nearby non-neuronal cells, which raises the possibility of local activation of $VMPO^{LPS}$ neurons by secreted immune molecules from glial

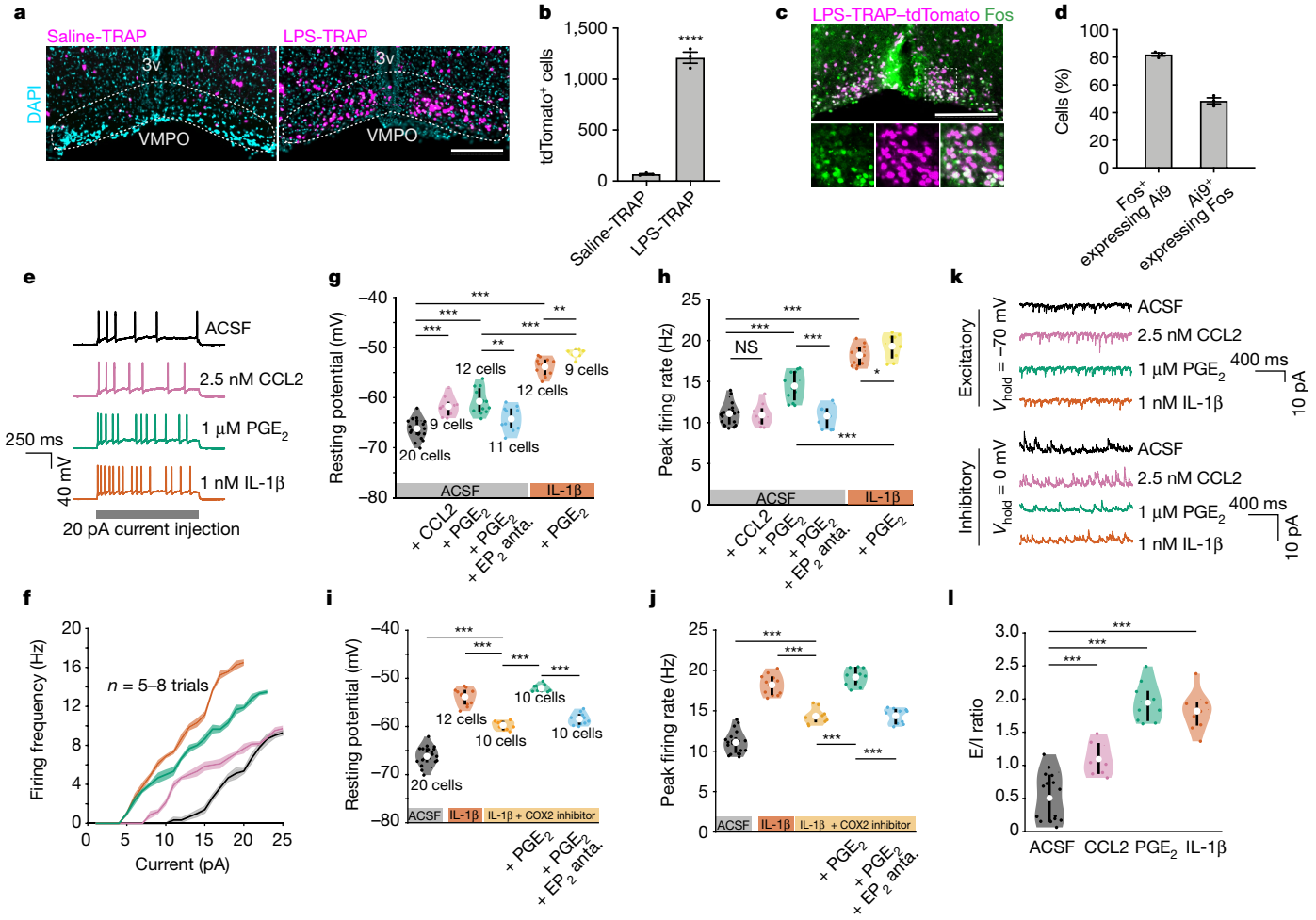

Fig. 2 | Effect of CCL2, PGE_2 and IL-1β on intrinsic and synaptic properties of $VMPO^{LPS}$ neurons. a, Reporter expression in the VMPO following saline-TRAP or LPS-TRAP. 3v, third ventricle. **b**, Average number of tdTomato$^+$ cells in the VMPO. $n = 3$ per group, Student's t-test, $^{****}P = < 0.0001$. **c**, Overlap of LPS-TRAP neurons and subsequent LPS-induced Fos expression. **d**, Mean per cent of signal overlap in **c**. $n = 3$ per group. **e**–**j**, Intrinsic properties. **e**, Examples of current-clamp recordings of $VMPO^{LPS}$ neurons after control (ACSF), 2.5 nM CCL2, 1 μM PGE_2 or 1 nM IL-1β treatment. **f**, Firing rate as a function of current injection. Control, $n = 8$ trials; CCL2, $n = 5$ trials; PGE_2, $n = 5$ trials; IL-1β, $n = 7$ trials. **g**,**h**, Membrane resting potentials (**g**) and peak firing rates (**h**) of $VMPO^{LPS}$ neurons treated with control (black), CCL2 (pink), PGE_2 (green) and after addition of an EP_2 antagonist (anta.; blue) in the presence of PGE_2, IL-1β (orange) and IL-1β with additional PGE_2 (yellow). **i**,**j**, Resting membrane potentials (**i**) and peak firing rates (**j**) of $VMPO^{LPS}$ neurons after IL-1β (orange), addition of COX-2 inhibitor (light orange), addition of PGE_2 (light green) and addition of an EP_2 antagonist (light blue). **k**,**l**, Synaptic properties. **k**, Voltage-clamp recordings of $VMPO^{LPS}$ neurons treated with control (ACSF), CCL2, PGE_2 and IL-1β, showing mEPSCs (top) and mIPSCs (bottom). **l**, Changes in the E/I ratio for control (ACSF), CCL2 (mean = 1.10 ± 0.06, $P = 2.20 \times 10^{-4}$), PGE_2 (mean = 1.95 ± 0.09, $P = 1.77 \times 10^{-5}$) and IL-1β (mean = 1.82 ± 0.08, $P = 1.83 \times 10^{-5}$). See Extended Data Table 1 for all values and statistical tests. For violin plots, the mean is represented by the central white circle, the black line represents the interquartile range. All error bars represent the s.e.m. P values were calculated using two-sided Wilcoxon rank-sum test. $^*P < 0.05$, $^{**}P < 0.01$, $^{***}P < 0.001$ and NS, not significant ($P > 0.05$). See the 'Statistics and reproducibility' section of the Methods for precise n values. Scale bar, 200 μm (**a** and **c**).

and epithelial cells[4,5]. Indeed, MERFISH[13,14] analysis indicated that about 70% of activated ependymal cells were also located within 200 μm of the base of the brain, adjacent to $VMPO^{Gal/Amigo2}$ neurons (Fig. 1k and Extended Data Fig. 2c, d). Moreover, astrocytes were more likely to be *Fos*$^+$ near the midline both within the VMPO and more dorsally (Fig. 1k and Extended Data Fig. 2c, d). The close proximity between activated $VMPO^{LPS}$ neurons and secretory ependymal and astrocytes therefore suggest that $VMPO^{LPS}$ neurons may be activated by signals secreted from local non-neuronal populations.

To identify the molecular mechanisms that underlie $VMPO^{LPS}$ neuronal activation, we examined the expression of immune molecules and receptors previously implicated in fever and inflammation. Similar to previous studies[5,20–22], we found that prostaglandin-endoperoxide synthase 2 (PTGS2; also known as or COX-2), interleukin-1β (IL-1β) and chemokine ligand 2 (CCL2) were expressed near the VMPO (Extended Data Fig. 3a–c). Following LPS administration, *Ptgs2* was identified in endothelial and pericyte cells of nearby vasculature after 60 min and in microglia after 120 min (Extended Data Fig. 3j). By contrast, *Il1b* was found in ependymal cells and meningeal cells at the base of the brain after 60 min and in microglia after 120 min (Extended Data Fig. 3k). *Ccl2* was found in ependymal cells as well as in *Gfap*$^+$ astrocytes near capillaries (Extended Data Fig. 3c, l). These data suggest that epithelial cells may stimulate an initial immune signal that is later amplified by local microglia.

snRNA-seq data showed that neurons from cluster 19 expressed IL-1 receptor accessory protein (*Il1rap*) (Extended Data Fig. 1g), which is required for IL-1β signalling[23–25], and we confirmed expression of *Il1rap* by $VMPO^{LPS}$ neurons in situ (Extended Data Fig. 3e). Although the PGE_2 receptor EP_3 has been implicated in the generation of fever[11], we did not detect *Ep3* in cluster 19 (Extended Data Fig. 1g). However, snRNA-seq and in situ expression analyses identified expression of the PGE_2 receptor *Ep2* throughout the preoptic region, including by $VMPO^{LPS}$ neurons (Extended Data Figs. 1g and 3d, g–i). Finally, $VMPO^{LPS}$ neurons also

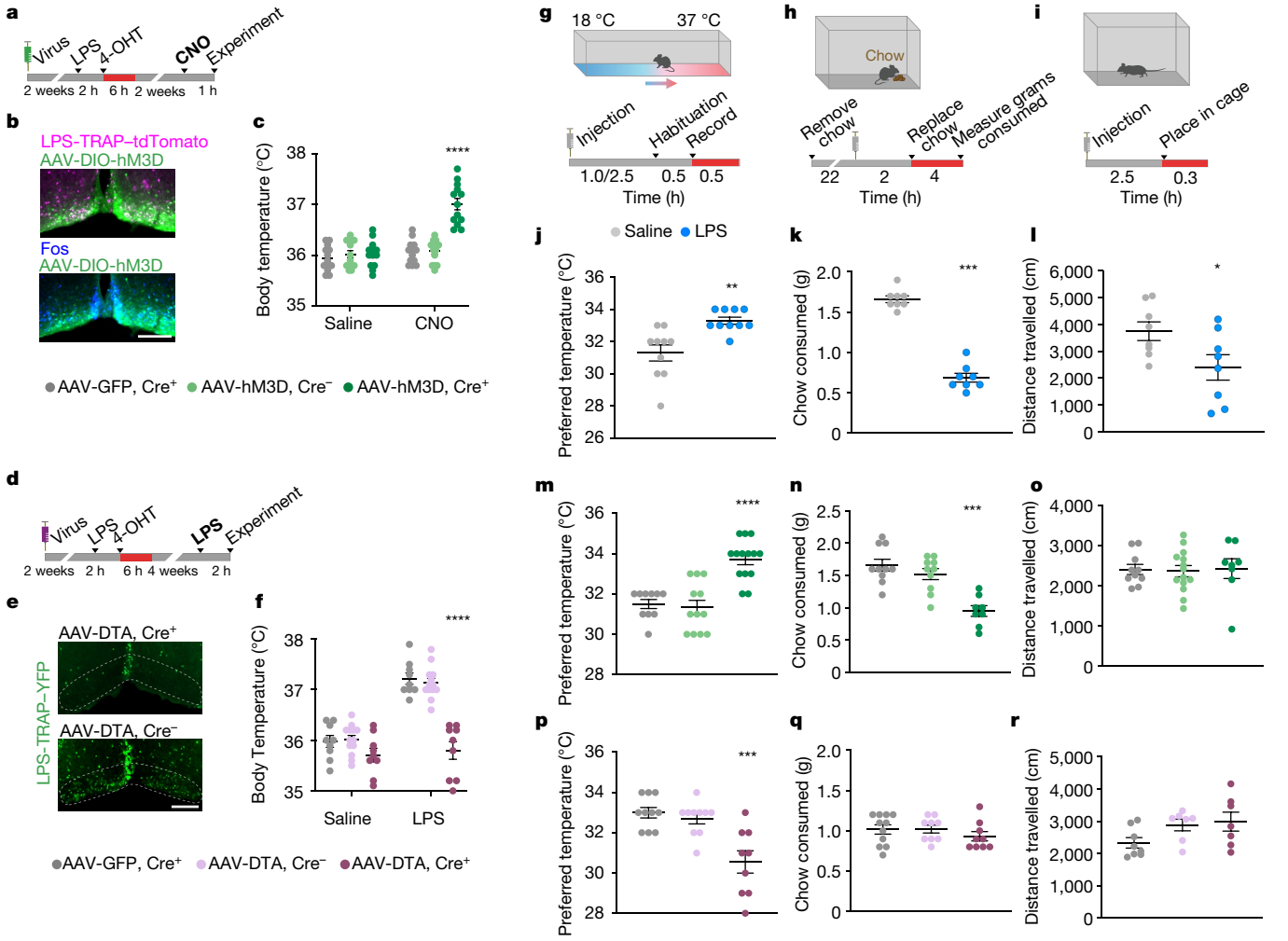

Fig. 3 | VMPO^{LPS} neurons drive LPS-induced generation of fever, warmth-seeking behaviour and appetite suppression. a, Experimental procedure for VMPO^{LPS} chemogenetic activation. **b**, Expression of chemogenetic activating receptor hM3D (green) in LPS-TRAP cells in the VMPO (magenta) and CNO-induced Fos expression (blue). **c**, Mean body temperature after saline or CNO injection in Cre$^+$ mice expressing hM3D, Cre$^-$ mice expressing hM3D or Cre$^+$ mice expressing GFP controls. Two-way ANOVA, $^{****}P < 0.0001$. **d**, Experimental procedure for VMPO^{LPS} cell-specific ablation by DTA. **e**, LPS-TRAP cells (green) in the VMPO after cell ablation (top) compared to control (bottom). **f**, Mean body temperature following saline or LPS injection in DTA-ablated mice and Cre$^-$ mice injected with AAV-DTA and Cre$^+$ mice expressing GFP controls, Two-way ANOVA, $^{****}P < 0.0001$. **g**–**i**, Schematics of the procedures used to test sickness behaviours: temperature preference (**g**), change in appetite (**h**) and change in locomotion (**i**). **j**–**l**, Quantification of behavioural changes in wild-type mice following saline or LPS injection. **j**, Median preferred external temperature, $^{**}P = 0.0016$. **k**, Mean appetite, $^{***}P < 0.0001$. **l**, Mean locomotion, $^{*}P = 0.0372$. $n = 8$ per group, two-tailed *t*-test. **m**–**o**, Quantification of behavioural changes following CNO injection in mice with activated VMPO^{LPS} neurons and controls (colours same as key in **b**). **m**, Median preferred temperature, $^{****}P < 0.0001$. **n**, Mean appetite, $^{***}P = 0.0007$. **o**, Mean locomotion. Kruskal–Wallis test with Dunn's multiple comparison. **p**–**r**, Quantification of behavioural changes in mice with ablation of VMPO^{LPS} neurons and controls (colours same as key in **e**). **p**, Median preferred temperature, $^{***}P = 0.0002$. **q**, Mean appetite. **r**, Mean locomotion. Kruskal–Wallis test with Dunn's multiple comparison. See the 'Statistics and reproducibility' section of the Methods for precise *n* values. All error bars represent the s.e.m. Scale bar, 200 µm (**b** and **e**).

expressed the receptor for CCL2 (*Ccr2*) (Extended Data Fig. 3f). Thus, VMPO^{LPS} neurons are probably sensitive to cytokines and prostaglandins released during infection and produced by nearby non-neuronal cells.

Immune activation of VMPO^{LPS} neurons

We next sought to determine the effect of CCL2, PGE_2 and IL-1β on VMPO^{LPS} neuron activity using the TRAP2 transgenic line, in which an inducible Cre-recombinase (2A-iCreER^{T2}) is inserted into the *Fos* locus[26,27]. To confirm that we could 'TRAP' (induce Cre expression in) LPS-activated neurons, TRAP2;Ai9 mice were injected with LPS and 4-hydroxytamoxifen (4-OHT), which induced significant expression of tdTomato in VMPO cells of LPS-treated TRAP (LPS-TRAP) mice compared with saline-treated TRAP (saline-TRAP) mice (Fig. 2a, b). We quantified the overlap of tdTomato$^+$ LPS-TRAP cells with Fos expression following a second LPS injection 2 weeks after the TRAP procedure. Similar to previous reports of TRAP2 labelling[26], 82% of Fos$^+$ cells in the VMPO were tdTomato$^+$, and 52% of tdTomato$^+$ cells expressed Fos (Fig. 2c, d), which indicated efficient and specific labelling of LPS-activated cells in TRAP2 mice.

Using tdTomato reporter expression in VMPO^{LPS} neurons of LPS-TRAP mice, we performed whole-cell patch clamp in live brain slices (Fig. 2e–j and Extended Data Fig. 4a, b). Application of CCL2 resulted in significant depolarization of VMPO^{LPS} neurons (Fig. 2g) and reduced rheobase current, which indicates an increased propensity of VMPO^{LPS} neurons to fire action potentials (Extended Data Fig. 4b and Extended Data Table 1), but had no impact on the peak firing rate (Fig. 2h). Application of PGE_2 or IL-1β also increased the excitability of VMPO^{LPS} neurons by depolarizing the membrane potential (Fig. 2g) and reducing the rheobase current

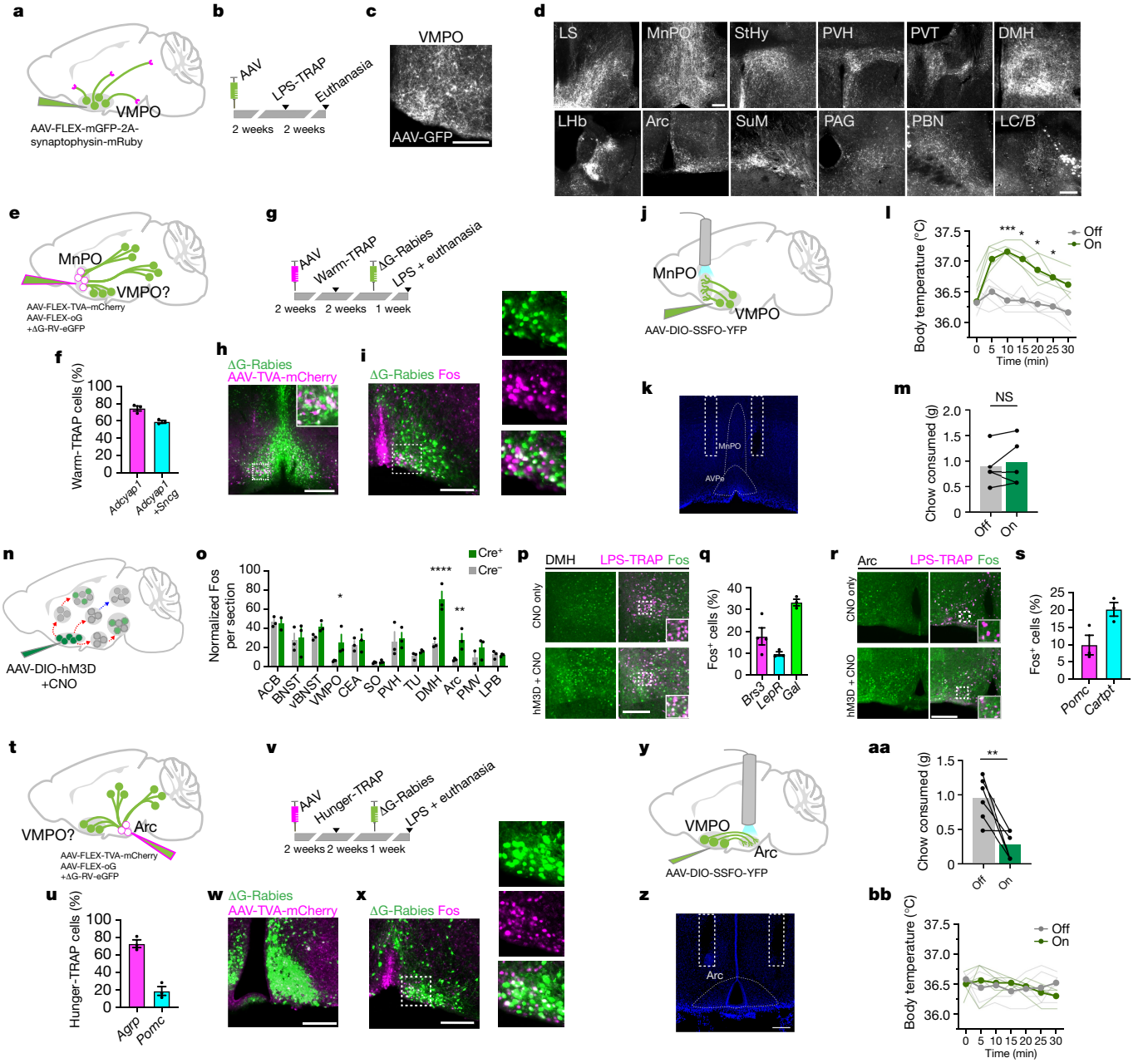

Fig. 4 | VMPO^{LPS} neurons regulate body temperature and appetite through direct and indirect synaptic connections. a–**d**, Anterograde circuit tracing. **a**,**b**, Anterograde tracing from LPS-TRAP neurons in the VMPO. **c**,**d**, Expression of GFP-labelled VMPO^{LPS} axonal fibres, $n = 6$ mice. **e**–**i**, Retrograde tracing from thermoregulatory neurons. **e**, Retrograde tracing from warm-sensitive neurons in AVPe/MnPO (warm-TRAP). **f**, Percent overlap of warm-TRAP neurons with *Adcyap1* and *Sncg*, $n = 3$. **g**, Experimental timeline for retrograde tracing. **h**, Starter cells in the AVPe/MnPO, green, G-deleted rabies, magenta, AAV-TVA–mCherry. **i**, Overlap of rabies-infected input cells (green) and LPS-induced Fos (magenta). Images on the right are magnifications of the boxed region. **j**–**m**, Optogenetic VMPO-MnPO terminal activation. **j**, Optogenetic activation of projections from VMPO^{LPS} neurons to the AVPe/MnPO. **k**, Fibre placement. **l**, Body temperature, stimulation (green) or no stimulation (grey) of VMPO^{LPS}-AVPe/MnPO projections. Light lines represent individual mice, dark lines represent the mean, $n = 5$, two-way ANOVA, $^{*}P < 0.05$, $^{**}P < 0.01$, $^{***}P < 0.001$. **m**, Chow consumed; dotted lines represent individuals, $n = 5$, two-way Mann-Whitney test. **n**–**s**, Identification of indirect target neurons. **n**, Schematic illustrating identification of downstream targets. **o**, Mean Fos expression following CNO treatment, $n = 3$ per group, two-way ANOVA, $P < 0.0001$. **p**, Fos expression in LPS-TRAP neurons, control (top), VMPO-activated (bottom). **q**, Mean marker expression in DMH LPS-TRAP neurons, $n = 3$ mice. **r**, Fos expression following CNO treatment. **s**, Mean marker expression in LPS-TRAP neurons in the Arc, $n = 3$ mice. **t**–**x**, Retrograde tracing from appetite-controlling neurons. **t**, Retrograde tracing from appetite-controlling neurons in the Arc. **u**, Overlap of *Agrp* and *Pomc* expression in hunger-TRAP neurons, $n = 3$ per group. **v**, Timeline of retrograde tracing. **w**, Starter cells in the Arc. **x**, Overlap of rabies-infected input neurons (green) and LPS-induced Fos (magenta). Images on the right are high magnifications of the boxed region. **y**–**bb**, Optogenetic VMPO-Arc terminal activation. **y**, Activation of VMPO^{LPS} projections to the Arc. **z**, Fibre placement. **aa**, Mean chow consumed following stimulation (on) or no stimulation (off) of VMPO^{LPS}-Arc projections, $n = 6$, $P = 0.0065$, two-way Mann–Whitney test. **bb**, Body temperature after VMPO^{LPS}-Arc stimulation ($n = 6$). All error bars represent the s.e.m. Scale bar, 200 µm (all images).

(Extended Data Fig. 4b). Moreover, PGE_2 or IL-1β application resulted in increased peak firing rates (Fig. 2h). PGE_2 application in the presence of IL-1β additively increased the excitability of VMPO^{LPS} neurons by further depolarizing the neurons (Fig. 2g), reducing the rheobase current (Extended Data Fig. 4b) and increasing the peak firing rate (Fig. 2h), which suggests that PGE_2 and IL-1β cooperatively enhance

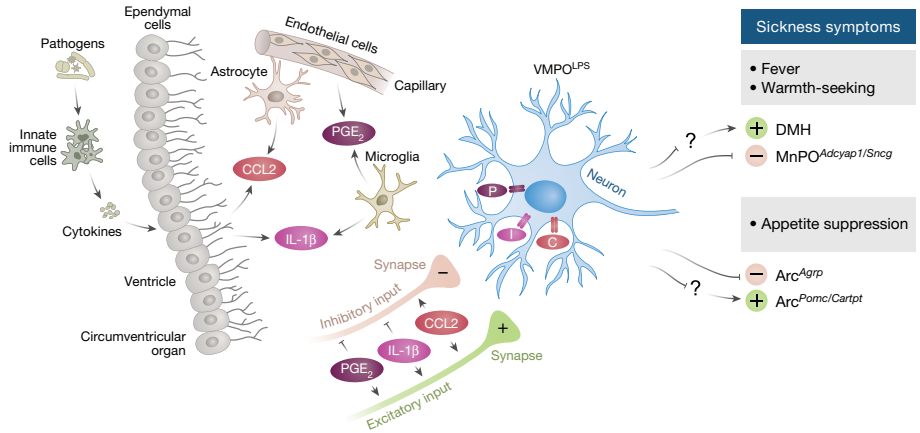

Fig. 5 | Model of the control of body temperature and appetite by VMPO^{LPS} neurons. Activation of the immune system in the periphery leads to circulating immune signals. These signals activate ependymal and endothelial cells lining the blood–brain barrier, which react by secreting additional signals, including IL-1β (I), PGE_2 (P) and CCL2 (C), which are further amplified by local glial cells. VMPO^{LPS} neurons are activated by these signals through their expression of the corresponding receptors as well as through activation of local synaptic inputs. In response, VMPO^{LPS} neurons induce fever, warmth-seeking and loss of appetite through direct and indirect connections to homeostatic brain circuits.

the excitability of VMPO^{LPS} neurons. The effects of PGE_2 were blocked by the addition of an EP_2 antagonist, thereby confirming a role for this receptor (Fig. 2g, h and Extended Data Fig. 4b).

IL-1β can enhance the biosynthesis of PGE_2 by inducing COX-2 (ref. [28]). Using a selective blocker of COX-2, IL-1β-mediated depolarization of VMPO^{LPS} was partially blocked (Fig. 2i, j and Extended Data Fig. 4c). This partial block was alleviated by the application of PGE_2, an effect that was abolished by an EP_2 antagonist (Fig. 2i, j and Extended Data Fig. 4c). This result suggests that IL-1β regulates intrinsic properties of VMPO^{LPS} neurons by directly increasing their excitability and indirectly by local PGE_2 biosynthesis. Consistent with this hypothesis, IL-1β receptor 1 (*Il1r1*) is expressed by endothelial cells, and COX-2 is induced in these cells after LPS administration (Extended Data Fig. 3j, m).

Next, we investigated the effect of CCL2, IL-1β and PGE_2 on synaptic inputs to VMPO^{LPS} neurons using voltage-clamp recordings to analyse miniature excitatory post-synaptic currents (mEPSCs) and miniature inhibitory post-synaptic currents (mIPSCs) (Fig. 2k and Extended Data Fig. 4d–k). Application of CCL2 increased the amplitude and frequency of mEPSCs (Extended Data Fig. 4d, e) and the frequency of mIPSCs (Extended Data Fig. 4f, g). By analysing the ratio of excitatory to inhibitory charge transfer (E/I ratio; Fig. 2l, Extended Data Fig. 4l, m and Extended Data Table 2), we found that CCL2 induces a net positive charge (Fig. 2l). Similarly, PGE_2 and IL-1β applications resulted in increased frequencies of mEPSCs (Extended Data Fig. 4e), decreased frequencies of mIPSCs (Extended Data Fig. 4i) and increased amplitudes of mIPSCs (Extended Data Fig. 4h). The effect of PGE_2 on mEPSCs was abolished by an EP_2 antagonist (Extended Data Fig. 4e). The E/I ratio showed that both PGE_2 and IL-1β resulted in a positive synaptic charge transfer to VMPO^{LPS} neurons (Fig. 2l). However, a COX-2 inhibitor abolished the effects of IL-1β (Extended Data Fig. 4f, g, j, k), which indicates that PGE_2 is required for the IL-1β-mediated changes in synaptic activity (Extended Data Fig. 4f, g, j, k). Together, these results show that PGE_2, IL-1β and CCL2 directly increase the excitability of VMPO^{LPS} neurons and indirectly increase excitatory input to VMPO^{LPS} neurons through changes in vesicle release and synaptic strengthening.

VMPO^{LPS} neurons generate fever

To determine whether VMPO^{LPS} neurons play a part in generating fever, we expressed the excitatory chemogenetic receptor hM3D in VMPO^{LPS} neurons of TRAP2 mice. The specificity of viral injections was verified post-mortem (Extended Data Fig. 5a), and we confirmed that clozapine-*N*-oxide (CNO) strongly activated hM3D-expressing VMPO^{LPS} neurons in slice preparations (Extended Data Fig. 6a–c). In vivo chemogenetic activation of TRAPed VMPO^{LPS} neurons significantly increased body temperature compared with controls (Fig. 3a–c). Similarly, chemogenetic activation of the VMPO in *Calcr*-Cre and *Gal*-Cre mice increased body temperature (Extended Data Fig. 5b). Thus, activation of VMPO^{LPS} neurons in the absence of inflammatory signals is sufficient to induce fever.

To test whether VMPO^{LPS} neurons are required for fever generation, we selectively ablated these neurons through the viral-mediated expression of Cre-dependent diphtheria toxin subunit A (DTA)[29] (Fig. 3d, e). Following VMPO^{LPS} neuron ablation, mice did not exhibit an increase in body temperature in response to LPS (Fig. 3f). Importantly, VMPO^{LPS} ablation did not affect the maintenance of normal body temperature, and VMPO^{LPS} ablation following saline-TRAP did not affect fever or temperature preference (Fig. 3f and Extended Data Fig. 5e–g). Thus, VMPO^{LPS} neurons are pivotal for fever generation.

The role of VMPO^{LPS} neurons in sickness

To determine whether VMPO^{LPS} neurons control other sickness behaviours, we quantified LPS-induced changes in preferred temperature, appetite and locomotion of the mice[30–32]. We found that 2.5 h after LPS injection, mice preferred an approximately 2 °C increase in external temperature, which was indicative of increased warmth-seeking behaviours (Fig. 3g, j). In addition, LPS-injected mice consumed about 60% less chow (Fig. 3h, k) and travelled about 40% less compared with controls, which indicated appetite suppression and increased lethargy, respectively (Fig. 3i, l).

To determine whether VMPO^{LPS} neurons affect warmth-seeking, appetite or lethargy behaviours, we chemogenetically activated VMPO^{LPS} neurons in TRAP2, *Gal*-Cre and *Calcr*-Cre mouse lines and then tested animals in each assay. VMPO^{LPS} neuron activation in TRAP2 mice resulted in increased preferred temperature and reduced appetite compared with controls, but no change in locomotion (Fig. 3m–o). Activating *Gal*$^+$ neurons significantly increased preferred temperature but did not affect appetite, whereas activating *Calcr*$^+$ neurons decreased appetite but did not affect preferred temperature (Extended Data Fig. 5c, d), which suggests that there is cell heterogeneity within the VMPO^{LPS} population. Indeed, although most LPS-induced Fos$^+$ neurons expressed either *Gal* or *Calcr*, a smaller subset was *Gal*$^+$*Calcr*$^+$ (Extended Data Fig. 1j), which highlights the advantage of the TRAP2 system to target all cell types activated by a given stimulus.

We next tested the requirement of VMPO^{LPS} neurons to induce sickness behaviours using DTA-mediated ablation. VMPO^{LPS}-ablated mice

no longer exhibited increased temperature preference after LPS administration, and there was no change in appetite or locomotion (Fig. 3p–r). The apparent lack of effect on appetite may be explained by a higher threshold of activated cells required to control appetite compared to warmth-seeking behaviour, or may result from additional circuits that control loss of appetite. Altogether, these results show that VMPO^{LPS} neurons are necessary and sufficient for warmth-seeking behaviour during sickness and sufficient to induce loss of appetite.

LPS-induced changes in thermoregulation

To determine the mechanisms by which VMPO^{LPS} neurons modulate homeostatic functions, we identified their downstream targets using a conditional virus expressing synaptophysin–mRuby and membrane bound-GFP that delineates synapses from fibres of passage (Fig. 4a–c). Projections to 12 brain areas were identified (Fig. 4d) that included areas related to stress and aversion as well as thermoregulation, appetite and sleep, thus representing possible nodes at which VMPO^{LPS} neurons may exert their function during sickness.

Next, we examined how VMPO^{LPS} neurons alter body temperature. Warm-sensitive neurons in the AVPe and MnPO decrease body temperature in response to warm external temperatures through connections with the dorsal medial hypothalamus (DMH), which leads to the inhibition of brown adipose tissue thermogenesis and behavioural thermoregulation[6]. To test whether VMPO^{LPS} neurons form direct connections with warm-sensitive neurons, we used Cre-dependent trans-synaptic retrograde rabies tracing from TRAPed warm-sensitive neurons (warm-TRAP) and measured retrograde rabies signals in VMPO^{LPS} neurons (Fig. 4e). Warm-TRAP neurons expressed the markers *Adcyap1* and *Sncg* for warm-sensitive neurons[6,13] (Fig. 4f and Extended Data Fig. 5h). We expressed the TVA receptor, optimized G protein and G-deleted rabies virus in AVPe/MnPO warm-TRAP cells (Fig. 4g, h) and found 38 ± 2.6% overlap between LPS-mediated Fos and retrograde rabies signal in the VMPO (Fig. 4i). This direct connectivity makes VMPO^{LPS} neurons ideally positioned to inhibit the activity of warm-sensitive neurons and thereby increase body temperature.

To confirm the functional connectivity between VMPO^{LPS} and warm-sensitive neurons, we optogenetically activated VMPO^{LPS}→AVPe/MnPO projections (Fig. 4j) using a stabilized step function opsin (SSFO) to reduce heat generated by extended light pulses[6,33]. Current clamp recordings showed that SSFO activation triggered long-lasting increases in firing frequency in VMPO^{LPS} neurons (Extended Data Fig. 6d–f). To test the function of VMPO^{LPS}→AVPe/MnPO projections in vivo, we implanted optic fibre cannulas above the AVPe/MnPO area (Fig. 4k). Following a 2-s laser pulse, mice exhibited a significant increase in body temperature, which peaked at around 10 min[6], but did not alter chow consumption (Fig. 4l, m). Altogether, these results show that VMPO^{LPS} neurons alter body temperature through inhibitory connections with warm-sensitive thermoregulatory neurons.

In addition to the VMPO, multiple brain areas were activated by LPS (Fig. 1c). To determine which of these brain areas are downstream of the VMPO circuit, we chemogenetically activated VMPO^{LPS} neurons and quantified the number of Fos$^+$ cells in LPS-activated brain regions (Fig. 4n, o). The thermoregulatory DMH[6] and appetite-controlling arcuate nucleus (Arc)[34] were significantly activated, with an almost 100% overlap between CNO-induced Fos and LPS-TRAP reporter expression (Fig. 4o, p, r). Activation of neurons expressing bombesin receptor 3 (BRS3) or leptin receptor (LEPR) in the DMH has been shown to increase body temperature, whereas silencing of DMH^{Brs3} neurons inhibits LPS-mediated fever[7,35]. Indeed, a substantial fraction of LPS-activated cells in the DMH expressed *Brs3* (18 ± 3.3%) and *Lepr* (10 ± 0.95%), whereas a large population (34 ± 2.6%) of LPS-sensitive DMH neurons expressed *Gal*, a population of unknown function (Fig. 4q). These data suggest that stimulation of VMPO^{LPS} neurons leads to the activation of DMH neurons involved in thermoregulation and metabolism.

LPS-induced changes in appetite

Next, we sought to determine whether VMPO^{LPS} neurons are directly connected to hunger-generating neurons (Fig. 4t). Neurons were TRAPed following food deprivation (hunger-TRAP), with the majority of hunger-TRAP Arc neurons expressing *Agrp*, whereas few expressed *Pomc*[34] (Fig. 4u and Extended Data Fig. 5i). Following rabies tracing from hunger-TRAP neurons, 22.5 ± 6% Fos$^+$ VMPO^{LPS} neurons were labelled by rabies virus, which indicated that VMPO^{LPS} neurons form direct inhibitory connections with Arc^{Agrp} neurons and therefore may cause loss of appetite during sickness (Fig. 4v–x). Optogenetic activation of those projections led to a substantial decrease in chow consumption following stimulation, whereas their body temperature remained unchanged (Fig. 4y–bb). Together, these data show that VMPO^{LPS} neurons decrease appetite through inhibitory projections to Arc^{Agrp} neurons.

Notably, the number of Fos$^+$ cells in the Arc following VMPO activation appeared higher than in controls (Fig. 4o, r). Because the Arc contains neurons that both induce and suppress appetite[34], we hypothesized that sickness may increase activity in appetite-suppressing neurons, which are characterized by *Pomc* and *Cartpt* expression[36,37]. Thus, we quantified the overlap between LPS-induced Fos expression and these markers in the Arc and found that Fos$^+$ cells expressed *Pomc* and *Cartpt* (Fig. 4s), which indicates that appetite-suppressing neurons in the Arc are probably indirectly activated following stimulation of VMPO^{LPS} neurons.

Summary

Altogether, our data showed that VMPO^{LPS} neurons are necessary and sufficient to generate fever, directly sense immune signals and coordinate sickness-induced increases in body temperature, warmth-seeking behaviour and appetite suppression. Owing to the location of activated non-neuronal cell populations and VMPO^{LPS} neurons near the OVLT, we propose that the activity in VMPO^{LPS} neurons is triggered by a paracrine mechanism generated by locally secreted immune signals (Fig. 5). Indeed, PGE_2, IL-1β and CCL2 are locally produced by ependymal and endothelial cells, as well as microglia and astrocytes, and these molecules increase the excitability of VMPO^{LPS} neurons through both direct changes of intrinsic properties and net increases in excitatory input. Circuit connectivity analysis and functional manipulations demonstrated how the activity of VMPO^{LPS} neurons leads to an increase in body temperature by directly inhibiting warm-sensitive neurons and through indirect multisynaptic activation of DMH$^{Brs3/Lepr}$ neurons, which in turn may activate brown adipose tissue thermogenesis and other thermoregulatory behaviours (Fig. 5). Furthermore, VMPO^{LPS} neurons formed direct inhibitory connections with appetite-increasing neurons to suppress feeding behaviour and showed indirect excitatory influence on appetite-suppressing neurons, which suggests a circuitry by which VMPO^{LPS} neurons may reduce appetite (Fig. 5). In addition, VMPO^{LPS} neurons projected to 12 brain areas, some of which are known to control thirst, pain sensation or social interactions, which suggests that other sickness behaviours may also be affected by VMPO^{LPS} neuron activity. On the basis of the data presented here, we propose that the function of VMPO^{LPS} neurons is to translate the peripheral inflammatory state into changes in brain activity to elicit sickness symptoms. Our results indicate that immune signals have an immediate effect on the excitability of VMPO^{LPS} neurons and plasticity in both VMPO^{LPS} neurons and their upstream synaptic partners in a locally coordinated fashion. Although there are probably other neuronal populations that control sickness symptoms, our study revealed that at least some of these behaviours are altered in a co-dependent manner, which reflects the need for coordinated changes in homeostatic systems to increase survival during infection.

Online content

Any methods, additional references, Nature Research reporting summaries, source data, extended data, supplementary information, acknowledgements, peer review information; details of author contributions and competing interests; and statements of data and code availability are available at https://doi.org/10.1038/s41586-022-04793-z.

1. Konsman, J. P., Parnet, P. & Dantzer, R. Cytokine-induced sickness behaviour: mechanisms and implications. *Trends Neurosci.* **25**, 154–159 (2002).
2. McCusker, R. H. & Kelley, K. W. Immune–neural connections: how the immune system's response to infectious agents influences behavior. *J. Exp. Biol.* **216**, 84–98 (2013).
3. Evans, S. S., Repasky, E. A. & Fisher, D. T. Fever and the thermal regulation of immunity: the immune system feels the heat. *Nat. Rev. Immunol.* **15**, 335–349 (2015).
4. Quan, N. & Banks, W. A. Brain–immune communication pathways. *Brain Behav. Immun.* **21**, 727–735 (2007).
5. Nakamori, T. et al. Organum vasculosum laminae terminalis (OVLT) is a brain site to produce interleukin-1β during fever. *Brain Res.* **618**, 155–159 (1993).
6. Tan, C. L. et al. Warm-sensitive neurons that control body temperature. *Cell* **167**, 47–59. e15 (2016).
7. Zhang, Y. et al. Leptin-receptor-expressing neurons in the dorsomedial hypothalamus and median preoptic area regulate sympathetic brown adipose tissue circuits. *J. Neurosci.* **31**, 1873–1884 (2011).
8. Zhao, Z. D. et al. A hypothalamic circuit that controls body temperature. *Proc. Natl Acad. Sci. USA* **114**, 2042–2047 (2017).
9. Elmquist, J. K., Scammell, T. E., Jacobson, C. D. & Saper, C. B. Distribution of Fos-like immunoreactivity in the rat brain following intravenous lipopolysaccharide administration. *J. Comp. Neurol.* **371**, 85–103 (1996).
10. Oka, T. et al. Relationship of $EP_{1\text{-}4}$ prostaglandin receptors with rat hypothalamic cell groups involved in lipopolysaccharide fever responses. *J. Comp. Neurol.* **428**, 20–32 (2000).
11. Lazarus, M. et al. EP3 prostaglandin receptors in the median preoptic nucleus are critical for fever responses. *Nat. Neurosci.* **10**, 1131–1133 (2007).
12. Machado, N. L. S., Bandaru, S. S., Abbott, S. B. G. & Saper, C. B. EP3R-expressing glutamatergic preoptic neurons mediate inflammatory fever. *J. Neurosci.* **40**, 2573–2588 (2020).
13. Moffitt, J. R. et al. Molecular, spatial, and functional single-cell profiling of the hypothalamic preoptic region. *Science* **362**, eaau5324 (2018).
14. Chen, K. H., Boettiger, A. N., Moffitt, J. R., Wang, S. & Zhuang, X. RNA imaging. Spatially resolved, highly multiplexed RNA profiling in single cells. *Science* **348**, aaa6090 (2015).
15. Butler, A., Hoffman, P., Smibert, P., Papalexi, E. & Satija, R. Integrating single-cell transcriptomic data across different conditions, technologies, and species. *Nat. Biotechnol.* **36**, 411–420 (2018).
16. Konsman, J. P., Tridon, V. & Dantzer, R. Diffusion and action of intracerebroventricularly injected interleukin-1 in the CNS. *Neuroscience* **101**, 957–967 (2000).
17. Kis, B. et al. Effects of LPS stimulation on the expression of prostaglandin carriers in the cells of the blood–brain and blood–cerebrospinal fluid barriers. *J. Appl. Physiol.* **100**, 1392–1399 (2006).
18. Zywitza, V., Misios, A., Bunatyan, L., Willnow, T. E. & Rajewsky, N. Single-cell transcriptomics characterizes cell types in the subventricular zone and uncovers molecular defects impairing adult neurogenesis. *Cell Rep.* **25**, 2457–2469.e8 (2018).
19. Roessmann, U., Velasco, M. E., Sindely, S. D. & Gambetti, P. Glial fibrillary acidic protein (GFAP) in ependymal cells during development. An immunocytochemical study. *Brain Res.* **200**, 13–21 (1980).
20. Duan, L. et al. PDGFRβ cells rapidly relay inflammatory signal from the circulatory system to neurons via chemokine CCL2. *Neuron* **100**, 183–200.e8 (2018).
21. Quan, N., Stern, E. L., Whiteside, M. B. & Herkenham, M. Induction of pro-inflammatory cytokine mRNAs in the brain after peripheral injection of subseptic doses of lipopolysaccharide in the rat. *J. Neuroimmunol.* **93**, 72–80 (1999).
22. Wilhelms, D. B. et al. Deletion of prostaglandin E2 synthesizing enzymes in brain endothelial cells attenuates inflammatory fever. *J. Neurosci.* **34**, 11684–11690 (2014).
23. Hojen, J. F. et al. IL-1R3 blockade broadly attenuates the functions of six members of the IL-1 family, revealing their contribution to models of disease. *Nat. Immunol.* **20**, 1138–1149 (2019).
24. Davis, C. J. et al. The neuron-specific interleukin-1 receptor accessory protein is required for homeostatic sleep and sleep responses to influenza viral challenge in mice. *Brain Behav. Immun.* **47**, 35–43 (2015).
25. Liege, S., Laye, S., Li, K. S., Moze, E. & Neveu, P. J. Interleukin 1 receptor accessory protein (IL-1RAcP) is necessary for centrally mediated neuroendocrine and immune responses to IL-1β. *J. Neuroimmunol.* **110**, 134–139 (2000).
26. Allen, W. E. et al. Thirst-associated preoptic neurons encode an aversive motivational drive. *Science* **357**, 1149–1155 (2017).
27. DeNardo, L. A. et al. Temporal evolution of cortical ensembles promoting remote memory retrieval. *Nat. Neurosci.* **22**, 460–469 (2019).
28. Molina-Holgado, E., Ortiz, S., Molina-Holgado, F. & Guaza, C. Induction of COX-2 and PGE_2 biosynthesis by IL-1β is mediated by PKC and mitogen-activated protein kinases in murine astrocytes. *Br. J. Pharmacol.* **131**, 152–159 (2000).
29. Wu, Z., Autry, A. E., Bergan, J. F., Watabe-Uchida, M. & Dulac, C. G. Galanin neurons in the medial preoptic area govern parental behaviour. *Nature* **509**, 325–330 (2014).
30. Kozak, W., Conn, C. A. & Kluger, M. J. Lipopolysaccharide induces fever and depresses locomotor activity in unrestrained mice. *Am. J. Physiol.* **266**, R125–R135 (1994).
31. Akins, C., Thiessen, D. & Cocke, R. Lipopolysaccharide increases ambient temperature preference in C57BL/6J adult mice. *Physiol. Behav.* **50**, 461–463 (1991).
32. Liu, Y. et al. Lipopolysacharide rapidly and completely suppresses AgRP neuron-mediated food intake in male mice. *Endocrinology* **157**, 2380–2392 (2016).
33. Yizhar, O. et al. Neocortical excitation/inhibition balance in information processing and social dysfunction. *Nature* **477**, 171–178 (2011).
34. Andermann, M. L. & Lowell, B. B. Toward a wiring diagram understanding of appetite control. *Neuron* **95**, 757–778 (2017).
35. Pinol, R. A. et al. Brs3 neurons in the mouse dorsomedial hypothalamus regulate body temperature, energy expenditure, and heart rate, but not food intake. *Nat. Neurosci.* **21**, 1530–1540 (2018).
36. Farzi, A. et al. Arcuate nucleus and lateral hypothalamic CART neurons in the mouse brain exert opposing effects on energy expenditure. *eLife* **7**, e36494 (2018).
37. Millington, G. W. The role of proopiomelanocortin (POMC) neurones in feeding behaviour. *Nutr. Metab.* **4**, 18 (2007).

Methods

Animals

Mice were maintained on a 12 h:12 h dark–light cycle with access to food and water ad libitum. The temperature was maintained at 22 °C and the humidity was controlled at 30–70%. All experiments were performed in accordance with NIH guidelines and approved by the Harvard University Institutional Animal Care and Use Committee. Owing to the high degree of neural activity elicited in the hypothalamus during social interactions, all mice were individually housed for 1 week before the start of experiments. As female mice show large natural fluctuations in body temperature linked to oestrus, which suggests that there is an additional mechanism for body temperature regulation, only male mice were used for experiments. C57BL/6J mice were used for fever induction, Fos expression analysis and cell-type identification experiments. TRAP2 transgenic mice (also called *Fos*$^{2A\text{-}iCreER}$)[26,27] are available from the Jackson Laboratory (stock number 030323). The Gal-Cre BAC transgenic line was imported from the Mutant Mouse Regional Resource Center (MMUCD 031060-UCD). Calcr-IRES-Cre mice were generated by the Gene Targeting and Transgenics Center at the Janelia Research Campus using accession number NM_001042725.1. The following transgenic reporter lines were obtained from the Jackson Laboratory: Ai9(RCL-tdT) (stock number 007909) and R26R-EYFP (stock number 006148). For all experiments, only mice heterozygous for TRAP2 and reporter constructs were used. Sample sizes were chosen on the basis of similar experiments from relevant studies.

Fever induction and body temperature monitoring

For intermittent temperature recordings, implantable temperature transponders (IPTT-300, Bio Medic Data Systems) were inserted under the skin below the neckline in the upper abdominal region to the right of the midline. Mice were anaesthetized using 2–4% isoflurane. Hair was shaved and skin was disinfected before transponder insertion. Mice recovered for 1 week before experiments. Fever was induced by an intraperitoneal injection of either LPS (50 μg kg^{-1}) or poly(I:C) (10 mg kg^{-1}). Mice were habituated in the experimental room in their home cage for 1 h before injection. Body temperature was measured hourly or immediately before behaviour experiments using a handheld transponder reader (DAS-7007, Bio Medic Data Systems). Statistical significance was measured using Kruskal–Wallis test to compare saline, LPS and poly(I:C) treatments. For continuous temperature monitoring, we implanted telemetry probes (E-Mitter G2, Starr Life Sciences) into the intraperitoneal space of anaesthetized mice. Body temperature was measured every 5 min for up to 24 h. To compare body temperatures of saline-treated versus LPS-treated groups in chemogenetic and ablation experiments, two-way analysis of variance (ANOVA) was used.

Warm challenge

Individually housed mice in their home cages were placed into a veterinary incubator set at 30 °C for 2 h with access to food and hydrogel, then euthanized for Fos expression analysis.

Single nuclear sequencing

The anterior ventral preoptic area was dissected from mice 2 h after administration of either saline or LPS. Dissected tissues from 5 mice were pooled for each sample, dounce homogenized on ice and centrifuged at 500*g* for 6 min at 4 °C. Supernatant was removed and passed through a 70-μm filter then through a 20-μm filter (MACS Smartstrainer) to remove large debris. DAPI was added to the suspension and nuclei were separated by FACS. The resulting suspension was loaded into a 10x Genomics Chromium single-cell chip at a concentration of about 500 nuclei per μl with the aim of sequencing 7,000–8,000 nuclei per sample. Downstream preparation of sequencing libraries was carried out using the 10x Genomics Single Cell Kit V2. The libraries were sequenced on an Illumina NextSeq500 instrument using instructions provided by 10x Genomics. Paired-end sequencing with read lengths of 150 nt was performed for all samples. Illumina sequencing reads were aligned to the mouse genome using the 10x Genomics CellRanger pipeline with the default parameters. Identification of cell-type clusters was performed as previously described[13]. In brief, we first filtered out non-nuclei such as mitochondria and red blood cells as well as obvious doublets. We selected variable genes using the Seurat command FindVariableGenes using *y* cut-off = 1, *x* low cut-off = 0.0125 and *x* high cut-off = 3. A total of 1,500 variable genes were collected from each sample, and the intersection of variable genes was used to perform canonical correlation analysis. Immediate early genes were removed from variable gene selection. Canonical correlation analysis was performed using 50 components with the aim of clustering similar cell types across the saline and LPS conditions. To generate cell clusters, we utilized the Jaccard–Louvain community detection approach in the Seurat command FindClusters with k.param = 15 and resolution set to 2. We used the following markers to identify major cell type classes: microglia (SELPLG^{+}), astrocytes (AQP4^{+}), immature oligodendrocytes (PDGFRA^{+}), mature oligodendrocytes (MAL^{+}) and ependymal cells (LRP2^{+}AQP4^{+})[13,18].

MERFISH

The MERFISH preoptic area probe libraries were designed and generated as previously described[13]. Mice aged 8–12 weeks were individually housed for 1 week. After 1 h of habituation, mice were injected with LPS (50 μg kg^{-1}); 2 h later, mice were euthanized and brains rapidly dissected and frozen in Tissue-Tek OCT (VWR) and stored at −80 °C before sectioning. The preoptic area was sectioned at −18 °C on a cryostat (Microm, HM550), generating 10-μm-thick coronal sections. Coverslips were treated and prepared as previously described[13]. In brief, beginning at approximately +0.5 bregma, slices staggered approximately 50 μm apart along the anterior–posterior (AP) axis were placed onto silanized 40 mm no. 1.5 coverslips pretreated with orange fiducial beads until slices spanning the extent of the VMPO had been collected. Sections were fixed in 4% paraformaldehyde (PFA), washed in PBS and dehydrated in 70% ethanol. Samples were stained with a hybridization mixture containing encoding probes for MERFISH measurements and for the non-combinatorial, sequential FISH measurements, and a poly(A) anchor probe, after which samples were embedded in a polyacrylamide gel matrix and cleared using SDS–proteinase K treatment, as previously described[13]. Samples were extensively washed with 2× SSC following digestion and stored at 4 °C in 2× SSC with 1:100 murine RNAse inhibitor for up to 1 week before imaging.

Samples were imaged as previously described, imaging the preoptic region from slices that contain the VMPO in three LPS-treated animals[13]. In brief, samples were stained with a readout hybridization mixture containing the readout probes for the first round of MERFISH measurements, along with a readout probe targeting the poly(A) anchor probe and DAPI to stain the cytoplasm and nucleus, respectively. Imaging was performed using a PlanApo ×60/1.3 NA silicon oil objective, taking a 9 × 9 grid of fields of view (FOV) that covers a 1.8 ×1.8 mm region centred on the preoptic region present in each tissue slice. Such a grid of fields of view was taken for each slice present on a given coverslip. The first round of imaging was performed in the 750 nm, 650 nm, 560 nm, 488 nm and 405 nm channels to image the Alexa-750 readout probe, the Cy5 readout probe, fiducial beads, the poly(A) probe and DAPI, respectively. Subsequent rounds of imaging were performed in the 750 nm, 650 nm and 560 nm channels only. After the first round of imaging, the sample was treated with TCEP to cleave the fluorescent dyes off the readout probes, hybridized with the readout probes for the second round of imaging, and then imaging was performed covering the same set of positions as the previous round. This process was repeated until rounds of imaging for both MERFISH and non-combinatorial, sequential FISH were completed. For all images of the fiducial beads, a single image at the surface of the coverslip was obtained. For the MERFISH

measurements of the 135 genes, poly(A) probe and DAPI imaging, seven 1.5-μm-thick *z*-stacks were collected. For the non-combinatorial sequential FISH measurements of the 20 genes, a single image at 4.5 μm above the coverslip surface was taken.

MERFISH image analysis was performed using algorithms and approaches similar to those previously described[13]. The revised pipeline used to perform the analysis is freely available at https://github.com/ZhuangLab/MERlin. The output of this pipeline is a cell by gene matrix of expression, wherein each gene targeted by MERFISH is represented as absolute RNA counts, and each gene targeted by non-combinatorial, sequential FISH is represented as the total fluorescence intensity of all pixels within the cell boundary. Counts were volume-normalized, and then data from each experiment were rescaled to reflect a typical counts density to minimize batch effects from different samples. Fluorescence intensities were normalized to the number of pixels contributing to each measurement, and then the background of each cell in the 650 nm and 750 nm channels were estimated as the median of all the non-combinatorial, sequential FISH measurements in that channel for a given cell (as no cell is expected to express more than a few of the 20 different genes analysed in this manner) and subtracted from the signal in each round of the corresponding colour. All data were then transformed as $\log_{10}(x+1)$. Cells without a segmentation boundary in the 4.5-μm *z*-plane were discarded owing to the absence of valid quantification for the non-combinatorial, sequential FISH genes. Additionally, cells were filtered on volume (discarding those with volumes less than 100 μm^3 or greater than 3,000 μm^3), MERFISH mRNA counts (discarding those with 20 or fewer total MERFISH counts) and high non-combinatorial, sequential FISH signals (discarding those yielding high signals in more than 5 genes; manual inspection suggested that these signals often arose from erroneous sources of signal).

Expression measurements from LPS-treated animals were normalized by calculating the *z*-score for each gene across all cells, and the same was done for the expression measurements previously collected from naive animals[13]. A single layer, 100 node neural net classifier was trained on the *z*-scored expression measurements of the naive animals using the 135 MERFISH genes measured by MERFISH and 20 genes measured by non-combinatorial, sequential multicolour FISH (Fos is not contained within these measurements) to predict the cluster label of each cell. The classifier was used to predict the cluster label for each cell in the LPS-treated data. Cells assigned to the 'ambiguous' class were discarded, as well as those with a prediction probability < 0.9. This left 92,990 of 204,319 cells with cluster assignments. A second round of classification was performed to recover unassigned LPS cells. In the second round, the assigned LPS cells were used to train a new single layer, 100 node neural net classifier to predict their assigned cluster labels. The classifier was then used to predict the unassigned cells in the LPS-treated data, again discarding predictions with probabilities < 0.9. A further 85,138 cells were assigned a cluster label, and the remaining 26,191 were labelled as ambiguous.

To identify neurons and neuronal clusters activated by LPS injection, the Fos signal of all cells assigned an inhibitory or excitatory cluster label was normalized by calculating the *z*-score for cells from each replicate independently. All neurons with a Fos signal that was 2 or more standard deviations greater than the mean Fos signal of all the cells in the same animal (that is, *z*-score ≥ 2) were considered Fos^+, and all other neurons were considered Fos^-. For cases in which non-neuronal cells were also analysed, the same procedure was used except that the *z*-score was calculated using all non-ambiguous cells. Clusters were determined to have significant enrichment of Fos^+ cells/neurons based on a binomial test and a false discovery rate of <5%. Measurements of distances of selected cell populations to the midline or base of the brain were calculated for the four slices with the most $VMPO^{Gal/Amigo2}$ cells in a given replicate, and data from all replicates were combined in the cumulative distribution function. *P* values were determined using Mann–Whitney *U*-test.

TRAP induction

4-OHT was dissolved to a concentration of 20 mg ml^{-1} in ethanol by shaking at 37 °C for 15 min then mixed with corn oil (Sigma) at a concentration of 10 mg ml^{-1} by vortexing. Ethanol was evaporated in a 37 °C oven for 1 h. The final 10 mg ml^{-1} 4-OHT solution was intraperitoneally injected into mice immediately after preparation at a dose of 50 mg kg^{-1}.

LPS-TRAP and saline-TRAP. Mice were habituated to the procedure room in their home cages for 1 h. Saline or LPS (50 μg kg^{-1}) was intraperitoneally administered, then 2 h later, prepared 4-OHT was administered. Mice were left in the same environment for an additional 4–6 h while 4-OHT is being metabolized and they recover from the fever. Although subsets of non-neuronal cells expressed Fos following LPS administration, we did not see any viral infection of non-neuronal cells following the TRAP procedure, presumably due to the use of neuronal-specific viral serotypes and promotors.

Warm-TRAP. Mice were placed in a 30 °C veterinary incubator for 2 h inside their home cages, then 4-OHT was administered. Mice remained in the incubator for an additional 4 h before returning to room temperature.

Hunger-TRAP. Mice were deprived of food for 22 h before 4-OHT administration. Regular chow was returned 6 h after 4-OHT injection.

Electrophysiology

Solutions. Modified artificial cerebrospinal fluid (ACSF), used as cutting solution, contained the following components (in mM): 105 choline chloride, 20 glucose, 24 $NaHCO_3$, 2.5 KCl, 0.5 $CaCl_2$, 8 $MgSO_4$, 5 sodium ascorbate, 3 sodium pyruvate, 1.25 NaH_2PO_4 (osmolarity of 290, pH 7.35). All recordings were conducted in oxygenated ACSF with the following composition (in mM): 115 NaCl, 2.5 KCl, 25 $NaHCO_3$, 1.25 NaH_2PO_4, 1 $MgSO_4$, 20 glucose, 2.0 $CaCl_2$ (osmolarity of 290, pH 7.35). See Extended Data Table 4 for more details.

The current-clamp internal solution contained the following components (in mM): 120 potassium gluconate, 2.0 sodium gluconate, 10 HEPES, 4.0 Mg-ATP, 2.0 Na_2-ATP, 0.3 Na_3-GTP and 4.0 NaCl (osmolarity of 292, pH 7.34). The voltage-clamp internal solution contained the following components (in mM): 130 D-gluconic acid, 130 cesium hydroxide, 5.0 NaCl, 10 HEPES, 12 di-tris-phosphocreatine, 1 EGTA, 3.0 Mg-ATP, 0.2 Na_3-GTP and 5 mM QX-314 (osmolarity of 291, pH 7.35). To visualize the neurons during recording, internal solutions contained 10 μM Alexa-488 or Alexa-594 as indicated. All chemicals were purchased from Sigma-Aldrich unless stated otherwise.

Acute brain slices. In vitro slice physiology was performed in adult TRAP2;Ai9 mice (aged 8–24 weeks) mice 2–10 weeks after TRAP induction. Slices were prepared using previously described methods[38]. Mice were lightly anaesthetized with isoflurane using a vaporizer (Datex-Ohmeda) connected to a clear acrylic chamber for 2 min, and then deeply anaesthetized with an intraperitoneal injection of a mixture of ketamine (100 mg kg^{-1}) and xylazine (10 mg kg^{-1}). Mice were transcardially perfused with ice-cold modified ACSF cutting solution, and brains were dissected into the same solution. Coronal slices (300-μm thick) were obtained using a vibratome (VT1000S, Leica) and collected in ice-cold cutting solution. VMPO was identified on the basis of its proximity to anatomical landmarks, including the ventricle and the ventral surface. $VMPO^{LPS}$ neurons were identified by the expression of the tdTomato reporter. After cutting, slices were incubated in oxygenated ACSF solution at 35 °C for 45 min and then at room temperature for the duration of the experiment.

In vitro recordings. Whole-cell current-clamp and voltage-clamp recordings were made using borosilicate glass patch pipettes (6–10 MΩ)

filled with current-clamp internal and voltage-clamp internal solutions, respectively, and slices maintained at 35 °C in oxygenated ACSF. Slices were visualized under custom-built infrared optics on a BX51WI microscope (Olympus Optical). Recordings were obtained with a Multiclamp 700B amplifier (Molecular Devices), and physiological data were collected using software written in LabView (National Instruments) and pClamp 10.3 (Molecular Devices). Current-clamp and voltage-clamp recordings were low-pass filtered at 1–2 kHz and digitized at 10–20 kHz. Membrane resting potentials were recorded 5 min after breaking into the cells. For rheobase current calculations, neurons were injected with increasing steps 1 pA (2 s of duration) until a single action potential was evoked in the recorded neuron. The same protocol with 1 pA steps (2 s of duration) was used to measure the peak firing rates of the neuron. For measurements of synaptic currents, voltage-clamp recordings were performed using a holding potential (−70 mV) that was near the reversal potential for chloride to record the excitatory currents. Similarly, to record the inhibitory currents, voltage-clamp recordings were perform using a holding potential (0 mV) that was near the reversal potential for AMPA and NMDA. Synaptic current measurements were performed in the presence of 1 μM TTX to block sodium currents.

Pharmacology. To synaptically isolate the neurons during current-clamp recordings, synaptic blockers (20 μM AP-5, 50 μM CNQX and 20 μM gabazine) were added to the bath solution. Similarly, to isolate miniature EPSCs and IPSCs, we used 1 μM TTX in the bath solution during voltage-clamp recordings.

Effects of PGE_2 and CCL2. During the current-clamp and voltage-clamp recordings, bath application of 1 μM PGE_2 and 2.5 nM CCL2 was used to determine the role of the abovementioned chemicals on the intrinsic properties and synaptic activities of $VMPO^{LPS}$ neurons. To analyse the contribution of EP_2 receptors, we used a selective EP_2 receptor antagonist (PF 04418948). Measurements were made 5–10 min after the start of perfusion of the drug.

Effects of IL-1β and NS-398. To analyse the role of IL-1 qualitatively and quantitatively, we incubated slices for 1 h in regular ACSF at 35 °C in the presence of 1 nM IL-1β. To selectively block the activity of COX-2, we incubated slices in the presence of 1 nM IL-1β and a selective COX-2 inhibitor (20 μM NS-398) for 1 h. During our experiments involving whole-cell patch recording, the same concentrations of IL-1β and NS-398 were continuously perfused through the recording chamber.

Optogenetic validation. TRAP2 mice (aged 8–16 weeks) were injected with 80–100 nl of AAV5-EF1a-DIO-hChR2(C128S/D156A)-EYFP (UNC Vector Core). Two to 8 weeks after TRAP induction, mice were killed, and brain slices (300-μm thick) were made as described above. We used a custom-built set-up to deliver a single 20-ms pulse of blue light (460 ± 10 nm, CBT-90-B-L11, Luminus) to activate hChR2(C128S/D156A) and used a single 50-ms green (525 ± 9 nm, CBT-90-B-L11, Luminus) light pulse to inactivate it.

Chemogenetic validation. TRAP2 mice (aged 8–16 weeks) were injected with 100 nl of AAV8-hSyn-DIO-hM3D(Gq)-mCherry virus (Addgene). Two to 8 weeks after TRAP induction, mice were killed, and brain slices (300-μm thick) were made as previously described. CNO (1–10 μM) was applied to the bath solution during whole-cell current clamp recordings.

Analysis. We used custom-written software (Matlab R2017a) to measure the timing of action potentials and the firing rates of neurons. Template match algorithm in Axograph (1.7.6) was used to measure the amplitude, timing and inter-event intervals of synaptic events. We used variable amplitude templates with τ_{rise} = 0.5 ms and τ_{decay} = 2 ms for the excitatory events and τ_{rise} = 2 ms and τ_{decay} = 5 ms for the inhibitory events.

Statistical test. Two-sided Wilcoxon rank-sum test in Matlab (R2017a) was used to compare the distribution.

Behaviour assays

Mice were individually housed for at least 1 week before testing, unless otherwise noted. To avoid activity-related fluctuations in body temperature, experiments were conducted during the light phase when mice are less active (exceptions are stated below). For all behaviours, mice were tested with saline, LPS and CNO in a randomized order. No difference was found with respect to the order of the trials. Animals were tested for a single behaviour per session with at least 1 week between trials. To avoid adapted responses to LPS, mice were not subjected to more than three LPS trials. All mice were habituated for 1 h before trials to minimize stress-induced temperature fluctuations. Statistical differences between groups were analysed using two-way ANOVA for body temperature tests or with non-parametric Kruskal–Wallis test with Dunn's multiple comparison for behavioural tests. N = 8–13 per group depending on the assay (see the main text, figure legends and graphs, with individual dots representing each mouse). For chemogenetic experiments, mice were used for multiple behaviour experiments, allowing 4–7 days between CNO injections to facilitate complete metabolism of CNO. Repeated CNO injections resulted in similar body temperatures for an individual mouse for each trial. For ablation experiments, mice were used for only one behavioural trial to circumvent adaptation to LPS administration.

Temperature preference. Mice were placed in a thermal gradient test box (Bio-TGT2, Bioseb) with one side set to 4 °C and the other side set to 55 °C either 1 h or 2.5 h after injection (CNO and LPS, respectively), depending on the experiment. Mice were given 30 min to habituate then recorded for 30 min. The time spent in temperature zones between 18 and 37 °C was recorded and analysed using Thermal Gradient Test software (Bioseb). The median temperature zone was used as the preferred temperature.

Feeding behaviour. Mice were deprived of food for 22 h before the experiment. After 1 h of habituation, mice were injected with saline, LPS or CNO, then a pre-weighed amount of regular chow was returned to the cage at the time of fever induction. The weight of remaining chow was measured 4 h later.

Locomotion. After 1 h of habituation and fever induction, mice were placed in a new cage and recorded for 10 min. Tests were recorded using a Geovision surveillance system, and the distance travelled was measured using Ethovision XT 8.0 (Noldus Information Technology).

Inter-male aggression. One hour after the onset of the dark cycle, under dim red lighting, castrated C57Bl6/J males (aged 6–8 weeks) swabbed with intact adult male urine (100 μl) were introduced into the home cage of an adult virgin male mouse (age of about 8 weeks). Mice were euthanized for tissue collection 30 min following aggressive attacking of the intruder, which was characterized by rapid bouts of biting leading to defensive reactions by the intruder (rearing and escaping). Intruder males were removed from the cage 10 min after the commencement of the first attack.

Male mating. Ovariectomized female mice (aged 6–8 weeks) were hormonally primed to be in oestrous as previously described[13]. On the test day, females were introduced into the home cage of an adult virgin male mouse (age of about 8 weeks) 1 h after the onset of the dark cycle, under dim red lighting. Male mice were euthanized for tissue collection 30 min following intromission of the female. Female mice were removed from the cage 10 min after the first intromission.

Male parenting. Virgin male mice were paired with females (age of about 7 weeks) and co-housed until the birth of pups (about 21 days). Fathers were allowed to remain with pups for 3 days before removal. Two days later, parental behaviour was tested. After 1 h of habituation, 1 h after the onset of the dark cycle, under dim red lighting, a single mouse pup (age 2–3 days) was introduced into one corner of the home cage away from nesting material. A parental response was defined as retrieval of the pup to the nest combined with nesting, crouching, grooming and licking behaviours. Fathers were euthanized for tissue collection 30 min following the retrieval of the pup to the nest. Only mice displaying all of the above behavioural subroutines were selected for further processing.

Chemogenetics

TRAP2 mice (aged 8–16 weeks) were used for these experiments. We injected 100 nl of AAV8-hSyn-DIO-HA-hM3D(Gq)-IRES-mCitrine virus (Duke Viral Vector Core) bilaterally into the VMPO (A–P: +0.1; medial–lateral (ML): ±0.15; dorsal–ventral (DV): −5.2) using a Drummond Nanoject III. Mice recovered for 2 weeks before TRAP (CreER) induction or mock induction. Two weeks after Cre induction, mice were intraperitoneally injected with 0.5 mg kg^{-1} CNO dissolved in saline. Temperature was recorded or behaviour was measured 1 h following CNO injection. Two-way ANOVA was used to compare experimental and control groups. In the figures, individual dots in graphs represent a mouse. Mice were used for multiple behaviour experiments, allowing 4–7 days between CNO injections to facilitate complete metabolism of CNO. Repeated CNO injections resulted in similar body temperatures for an individual mouse for each trial, regardless of the experimental condition.

Optogenetics

TRAP2 mice (aged 8–16 weeks) were injected with 80–100 nl of AAV5-EF1a-DIO-hChR2(C128S/D156A)-EYFP (SSFO; UNC Vector Core) bilaterally into the VMPO (AP: +0.1; ML: ±0.15; DV: −5.2) using a Drummond Nanoject III. Optic fibres (Doric Lenses) were then implanted above the AVPe/MnPO (AP: +0.5; ML: ±0.3; DV: −4.6) or the Arc (AP: −1.5; ML: ±0.4; DV: −5.5). Fibres were cemented to the skull. Mice recovered for 2 weeks before LPS-TRAP (CreER) induction. Two weeks after Cre induction, mice underwent a habituation and testing protocol specific to the behavioural test (see below). Optogenetic stimulation was a single 2 s constant blue LED stimulation. The light intensity at the tip of the dual fibre was measured before each testing day and adjusted to about 10 mW. For the body temperature test, mice were habituated to the optogenetic set-up with the fibre connected for 1 h on three consecutive days. On the fourth day, mice were habituated for 30 min, then half of the mice underwent the 'light off' behavioural testing and half underwent the 'light on' testing. Body temperature was measured before stimulation and then every 5 min. On the fifth day, mice underwent the opposite (on versus off) trials (30 min habituation and 30 min body temperature measurements). No difference was found when comparing the order of the on or off trials, $n = 5$. For the appetite test, mice were habituated for 1 h for three consecutive days. Chow was removed from cages at 17:00 on the third day. On the fourth day, mice were habituated for 30 min, then half of mice underwent the light-on and half underwent the light-off trials. The weight of chow was measured before and after the 30 min trial. Mice were allowed 1 day to recover, and the following day (day 6) food was removed at 17:00. Day 7 mice underwent the opposite (on versus off) trial. No difference was found when comparing the order of on or off trials, $n = 6$. The placement of fibres was verified post-mortem, and those with incorrect fibre placements were removed from the study.

Cell ablation

AAV8-EF1a-mCherry-FLEX-dtA (UNC Vector Core) was stereotactically injected bilaterally into the VMPO of TRAP2 mice (100 µl) (AP: +0.1; ML: ±0.15; DV: −5.2) using a Drummond Nanoject III. Mice recovered for 2 weeks and then underwent LPS-TRAP induction. Body temperature response to LPS or saline treatment or behaviour analyses were conducted 4–5 weeks later. The accuracy of virus injection as complete or near-complete loss of reporter-positive cells in the VMPO was used to determine the success of ablation and subsequent inclusion for analysis. Two-way ANOVA was used to compare experimental and control groups. Individual dots in graphs represent each mouse. Mice were used for only one behavioural trial to circumvent adaptation to LPS administration.

Anterograde tracing

AAVDJ-hSyn-FLEX-mGFP-2A-synaptophysin-mRuby (Stanford Vector Core) was stereotaxically injected bilaterally into the VMPO (AP: +0.1; ML: ±0.15; DV: −5.2) using a Drummond Nanoject III (100 nl) into adult TRAP2 mice. After 2 weeks, mice underwent TRAP/Cre induction, and after an additional 2 weeks for viral/fluorophore expression, mice were transcardially perfused with 4% PFA. Tissue was cryoprotected (30% sucrose) and serial sections prepared using a freezing microtome (50 µm). Sections were mounted onto Superfrost plus slides, coverslipped with Vectashield plus DAPI and imaged at ×10 magnification using AxioScan and Zen Blue 3.4 software (Zeiss).

Monosynaptic input tracing

A 1:1 ratio (100 nl) of AAV1-EF1a-FLEX-TVA-mCherry (avian TVA receptor, UNC Viral Vector Core) and AAV1-CAG-FLEX-oG-WPRE-SV40-PA (optimized rabies glycoprotein, Salk Institute) was stereotaxically injected into either the AVPe/MnPO (bregma coordinates AP: +0.5; ML: ±0.2; DV: −5.0) or Arc (AP: −1.5; ML: ±0.2; DV: −5.8) of adult TRAP2 mice. Two weeks later, TRAP/Cre was induced, and then 1 week later, G-deleted rabies virus (deltaG-RV-eGFP, Janelia Viral Tools Facility) (200 nl) was injected into the same coordinates. Seven days later, mice were transcardially perfused with 4% PFA. Tissue was post-fixed in PFA overnight and cryoprotected (30% sucrose), then serial sections were prepared using a freezing microtome (50 µm). Sections were imaged at ×10 using AxioScan (Zeiss).

In situ hybridization

Double-label and triple-label FISH was performed using a RNAscope assay V1 kit (Advanced Cell Diagnostics (ACD)) according to the manufacturer's instructions with a few exceptions. Freshly frozen brains were sectioned using a cryostat at 16 µm and stored at −80 °C. Slides were thawed and fixed in 4% PFA for 15 min followed by dehydration in 50%, 75% then 100% ethanol. Cells were permeabilized for 30 min at room temperature using Protease III provided by ACD. Sections were then processed as suggested by the ACD protocol. Slides were imaged at ×20 on an Axioimager Z2 using Axiovision Release 4.8 (Zeiss). All probes were made by ACD. Quantification of marker expression was done using an adapted CellProfiler v.2.2 (Broad Institute) pipeline that identified cells using the DAPI signal and identified cells with fluorescent signals corresponding to Fos and specific marker genes.

Immunohistochemistry

To visualize Fos protein, perfused tissue was sliced using a freezing microtome at 50 µm. Sections were then incubated in blocking solution containing 5% goat serum, 3% FBS and 0.3% TritonX-100 diluted in PBS for 1 h at room temperature. Primary antibodies rabbit anti-Fos (9F6, Cell Signaling) and chicken anti-GFP (ab13970, Abcam) were diluted 1:1,000 in blocking solution, and sections were incubated overnight at 4 °C. After rinsing with PBS, secondary antibodies were applied at 1:1,000 dilution in PBS for 2 h at room temperature. Secondary antibodies used included Alexa-488 anti-rabbit (A21206, Invitrogen), Alexa-568 anti-rabbit (A11011, Invitrogen), Alexa-647 anti-rabbit (A21245) and Alexa-488 anti-chicken (A32921, Invitrogen). Sections were rinsed in PBS, mounted onto Superfrost plus slides, coverslipped with

Vectashield containing DAPI and imaged on a Axioscan at ×10 (Zeiss) at 0.65 μm pixel^{-1}. Fos^{+} cell nuclei were identified algorithmically in serial section images by spatial filtering, thresholding and finding connected components. Spots of connected pixels ranging from approximately 30 to 315 μm^2 (6.5–20 μm diameter) were counted as Fos^{+} nuclei. Contours of brain areas were manually drawn, aided by local architecture and landmarks and an atlas of the mouse brain. Brain areas were measured in each section for three mice per group. Statistical significance between LPS-treated and saline-treated groups was determined using two-way ANOVA with Fisher's test for multiple comparisons.

Statistics and reproducibility

Statistical differences between groups were analysed using two-way ANOVA for body temperature tests or with non-parametric Kruskal–Wallis test with Dunn's multiple comparison for behavioural tests. Use of other statistical tests are noted in the figure legends. All statistical tests are two-sided. See Extended Data Tables 5 and 6 for precise animal and cell numbers for Figs. 2 and 3 and Extended Data Fig. 4.

Antibody staining with Fos in the VMPO (Fig. 1e–g and Extended Data Fig. 1b, c) was repeated independently three times, with similar results obtained. Visualization of reporter expression in the VMPO of saline-TRAP and LPS-TRAP mice for the purpose of quantification was repeated independently two times (one to two mice each) (Fig. 2a). Visualization of projection patterns from VMPO neurons was repeated independently four times, with similar results obtained (Fig. 4c, d). Retrograde rabies tracing from warm-sensitive neurons and appetite-controlling neurons was repeated independently two times, with similar results obtained (Fig. 4h, i, w, x). Identification of indirect target neurons was repeated independently two times, with similar results obtained (Fig. 4o–s). All RNAscope experiments were repeated independently three separate times, with similar results obtained (Extended Data Figs. 3 and 4h, i).

Reporting summary

Further information on research design is available in the Nature Research Reporting Summary linked to this paper.

Data availability

Raw and processed data have been deposited in the Gene Expression Omnibus and are available under accession number GSE197547.

Code availability

The pipeline used to perform MERFISH analyses is freely available at https://github.com/ZhuangLab/MERlin. Other custom code is available upon request.

38. Kapoor, V., Provost, A. C., Agarwal, P. & Murthy, V. N. Activation of raphe nuclei triggers rapid and distinct effects on parallel olfactory bulb output channels. *Nat. Neurosci.* **19**, 271–282 (2016).

Acknowledgements We thank K. Prichett-Corning and other veterinary staff at the Harvard Office of Animal Resources for advice on working with sick mice; R. Hellmiss and staff at MCB Graphics for help with illustrations; A. Emery and J. Emery for assistance with histology and RNAscope experiments; members of the Dulac laboratory for helpful advice on experiments, analysis and the manuscript; and F. Engert and R. Losick for comments on the manuscript. This work was supported by NIH awards K99NS114107 to J.A.O. and F31MH120911 to E.V., NIH grant R01NS050835 to L.L, and NIH grant R01NS112399 and Simons Foundation Award 572189 to C.D. C.D., X.Z. and L.L. are investigators at the Howard Hughes Medical Institute.

Author contributions J.A.O. and C.D. conceived and designed the study. J.A.O. performed and analysed tracing, chemogenetic and ablation experiments and associated behavioural assays. J.A.O., C.D., S.W.E. and X.Z. designed the MERFISH experiments and analysis. S.W.E. performed and analysed all MERFISH experiments. J.A.O. and D. Lee. generated cDNA libraries for the snRNA-seq experiments. D. Lee and E.V. performed the snRNA-seq analysis. V.K. performed electrophysiological experiments and analysis. J.A.O. and D. Liu performed the optogenetic experiments. J.D.M. wrote the Matlab program for Fos expression quantification. J.A.O. and D. Lee performed and analysed the immunohistochemistry and in situ hybridization experiments. L.A.D. and L.L. shared the unpublished TRAP2 transgenic mouse line. J.A.O. and C.D. wrote the manuscript with input from all authors.

Competing interests X.Z. is an inventor on patents applied for by Harvard University related to MERFISH.

Additional information
Supplementary information The online version contains supplementary material available at https://doi.org/10.1038/s41586-022-04793-z.
Correspondence and requests for materials should be addressed to Catherine Dulac.
Peer review information *Nature* thanks Jan Siemens and the other, anonymous, reviewer(s) for their contribution to the peer review of this work.
Reprints and permissions information is available at http://www.nature.com/reprints.

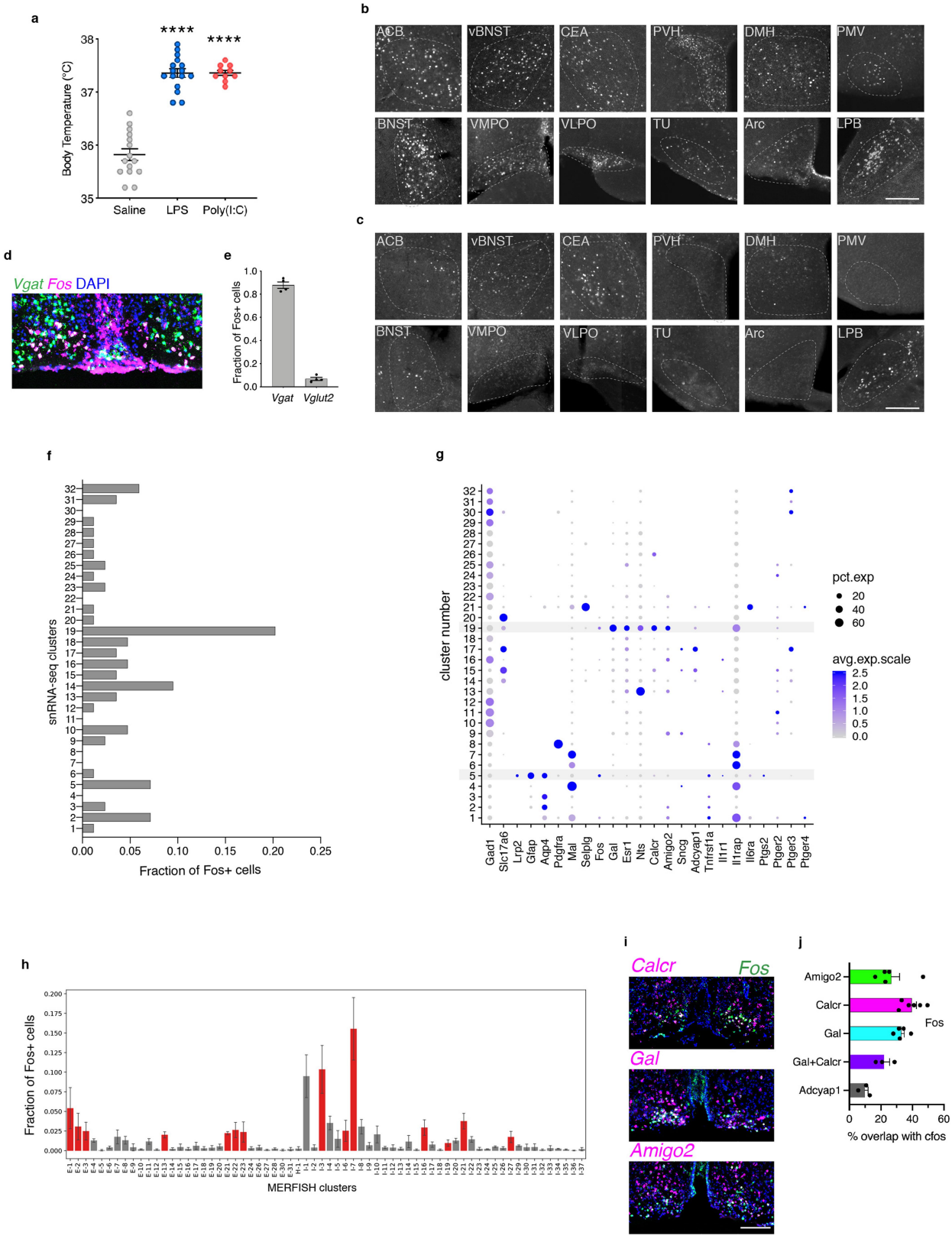

Extended Data Fig. 1 | See next page for caption.

Extended Data Fig. 1 | Specificity and identity of VMPO^{LPS} neurons during inflammation. (a) Mean body temperature 2 h following injection of saline (n = 13), LPS (n = 16) or Poly(I:C) (n = 10). (b-c) Representative images of Fos expression in brain areas displaying significant increases in number of Fos+ cells following LPS administration (b) or saline (c), scale bar for all panels = 200μm. (d) mRNA expression of inhibitory neuronal marker *Vgat* (green) and *Fos* (magenta) in the VMPO after LPS injection. (e) Fraction of *Fos*+ cells that express *Vgat or Vglut2* (n = 4). (f) Quantification of the fraction of *Fos*+ cells within individual snRNA-seq clusters in LPS-injected sample. (g) Dotplot of average expression of marker genes and genes with immunological significance in each cluster: dot size indicates percent of cells in cluster with measurable expression and color indicates average expression levels; ependymal cluster cluster #5 and neuronal cluster #19, found significantly activated after LPS injection are highlighted in red. (h) Quantification of the fraction of *Fos*+ cells in individual MERFISH neuronal clusters, with statically significant enrichment for *Fos*+ cells indicated in red, n = 3. (i) mRNA expression of markers for VMPO^{LPS} neurons (*calcR*, *gal* and *amigo2*) in LPS-injected mice. (j) Mean of overlap of markers for VMPO^{LPS} neurons and for warm-sensitive neurons (*adcyap1*) with LPS-mediated Fos expression in the VMPO, n = 3 mice/experiment. All scale bars = 200μm. All error bars = SEM.

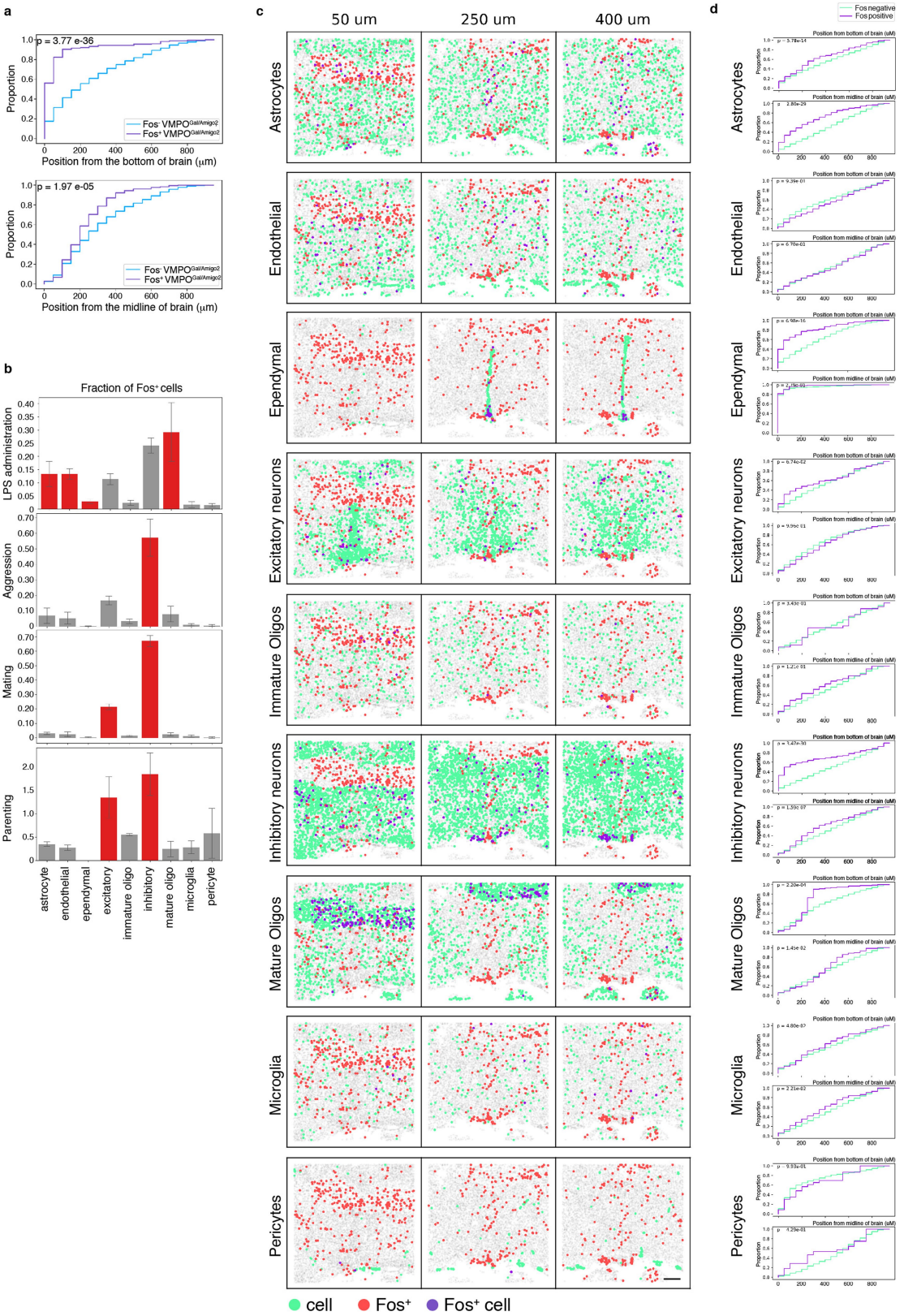

Extended Data Fig. 2 | Spatial distribution of activated neuronal and non-neuronal cell type classes in the preoptic area during inflammation. (a) Cumulative distribution of *Fos*+ (purple) and *Fos*- (blue) VMPO$^{Gal/Amigo2}$ neurons as a function of the distance to the bottom of the section (top) or the midline (bottom), n = 3 replicates. (b) MERFISH analysis indicating the fraction of *Fos*+ cells in major cell type classes in samples from mice injected with LPS versus mice displaying other behaviors: aggression, mating or parenting. Significantly activated populations are indicated in red. (c) Spatial distribution of major cell type classes in MERFISH analysis, cell type (green), *Fos*+ cell (red), *Fos*+ cells in the indicated cell type (purple). (d) Cumulative distribution of *Fos*+ (purple) and *Fos*- (green) cells in major cell type classes as a function of the distance to the bottom of the section (top) or the midline (bottom), n = 3 mice. All scale bars = 200μm. All error bars = SEM.

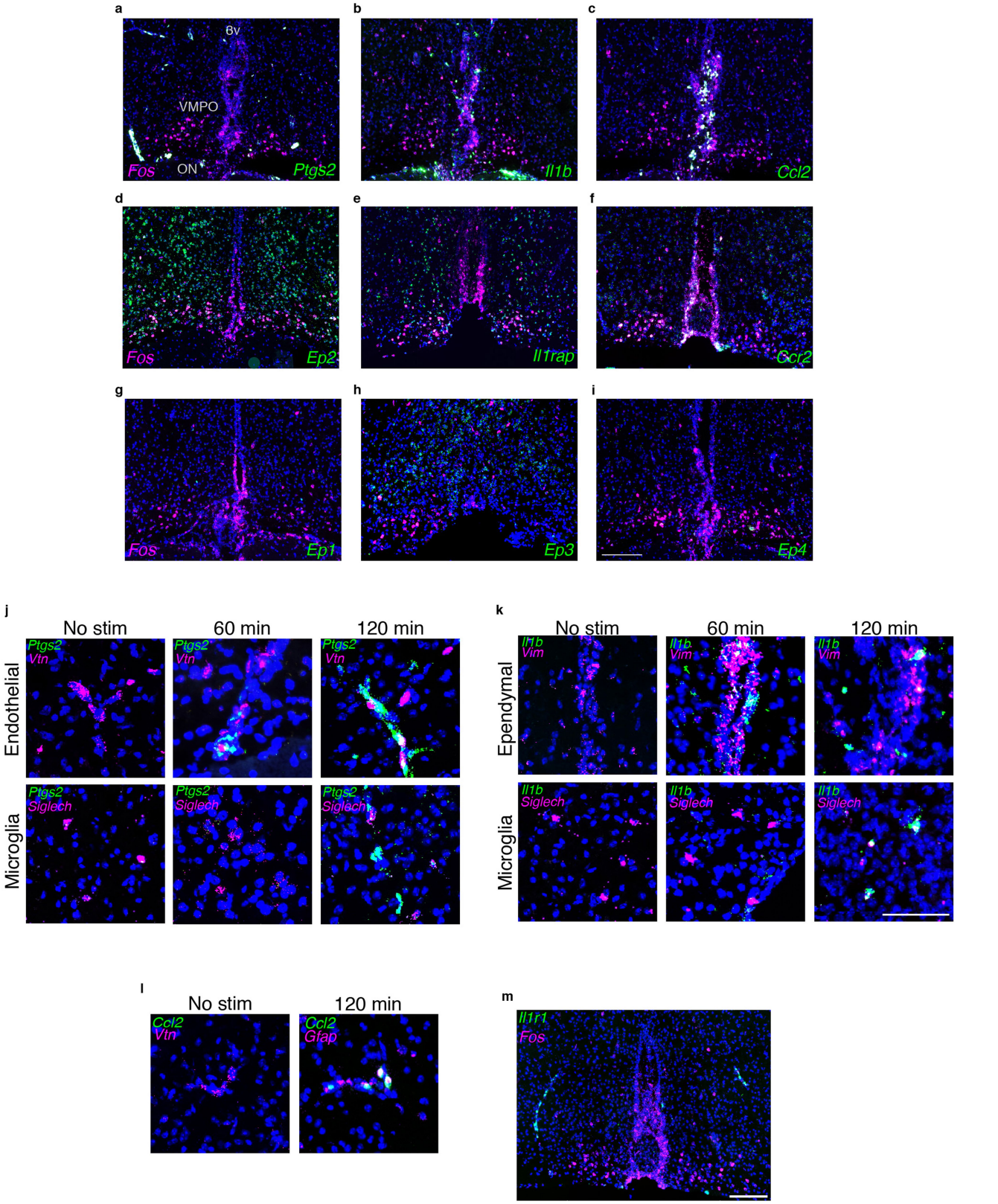

Extended Data Fig. 3 | Expression of key immune molecules and their receptors in the VMPO. (a-i) mRNA expression in the VMPO at 2hrs post LPS administration, genes of interest in green, LPS-induced Fos is in magenta. Scale bar for a-i = 200µm (a) Prostaglandin E synthase 2 (*ptgs2*) and its receptors *ep2* (d), *ep1* (g), *ep3* (h), *ep4* (i). (b) interleukin-1β (*il1β*) and its receptor *il1rap* (e). (c) chemokine ligand 2 (*ccl2*) and it's receptor chemkine receptor 2 (*ccr2*) (f). (j) Expression of *ptgs2* in absence of LPS stimulation and at 60min and 120min post LPS. No or weak expression is found without LPS stimulation, and expression after LPS challenge shows overlap with markers for endothelial cells and microglia. (k) Expression of *il1*β with no stimulation and at 60min and 120min post LPS, overlap with markers for ependymal cells and microglia. Scale bar for j-l = 50µm (l) Expression of *ccl2* with no stimulation and 120 min post LPS inejction, overlap with *gfap*+ astrocytes. (m) Expression of *il1r1* in the VMPO after LPS injection, Scale bar = 200µm.

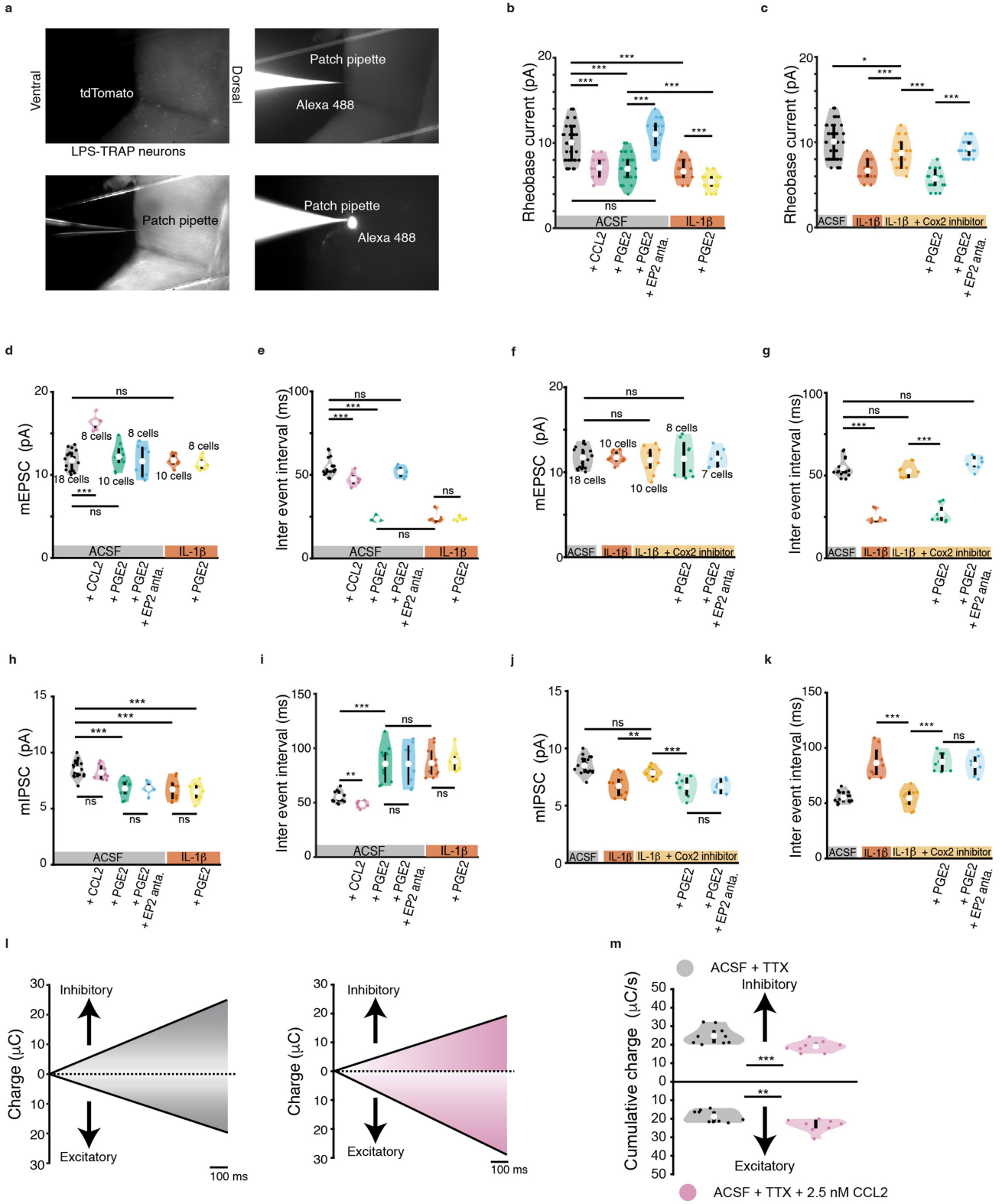

Extended Data Fig. 4 | See next page for caption.

Extended Data Fig. 4 | Effects of PGE-2 and cytokines on the intrinsic properties and synaptic activity of $VMPO^{LPS}$ neurons. (a) Wide field microscope images depicting tdTomato expression in the VMPO of TRAP2;Ai9 during whole cell patch clamp recording with pipette containing Alexa 488. (b) Changes in rheobase current for $VMPO^{LPS}$ neurons in presence of ACSF (black), CCL2 (pink), PGE2 (green), addition of EP2 antagonist in presence of PGE2 (blue), IL-1β (orange) and further addition of PGE2 (yellow), and (c) IL-1β (orange), addition of COX-2 inhibitor in the presence of IL-1β (light orange), further addition of PGE2 (light green) and further addition of EP2 antagonist (light blue). During whole cell voltage clamp recordings, changes in (d) amplitude of miniature EPSCs, (e) inter event interval for miniature EPSCs, (f) amplitude of miniature IPSCs and (g) inter event interval for miniature IPSCs for $VMPO^{LPS}$ neurons in presence of ACSF (black), CCL2 (pink), PGE2 (green), addition of EP2 antagonist in presence of PGE2 (blue), IL-1β (orange) and further addition of PGE2 (yellow). Changes in (h) amplitude of miniature EPSCs, (i) inter event interval for miniature EPSCs, (j) amplitude of miniature IPSCs and (k) inter event interval for miniature IPSCs for $VMPO^{LPS}$ neurons in the presence of IL-1β and COX-2 inhibitor (light orange), further addition of PGE2 (light green) and further addition of EP2 antagonist (light blue). (l) Cumulative plots showing total charge transferred over 1s for inhibitory events and excitatory events for control (black) and CCL2 (pink). (m, top) Cumulative charge transferred by IPSCs for control (mean value of 24.81 ± 0.14 μC/s) and CCL2 (mean value of 19.06 ± 0.09 μC/s $p = 2.0 * 10^{-03}$ for). (m, bottom) Cumulative charge transferred by miniature EPSCs for control (mean value of 18.81 ± 0.09 μC/s) and CCL2 (mean value of 23.37 ± 0.11 μC/s $p = 9.0 * 10^{-03}$). All other values and statistical tests are catalogued in Extended Data Table 2. For violin plots, central white circle depicts the mean value and thick black line depicts the interquartile range. All p values shown are for two-sided Wilcoxon rank sum test with * = $p < 0.05$, ** = $p < 0$, *** = $p < 0.005$ and ns = $p > 0.05$. All error bars = SEM. See Statistics and Reproducibility section for exact n values.

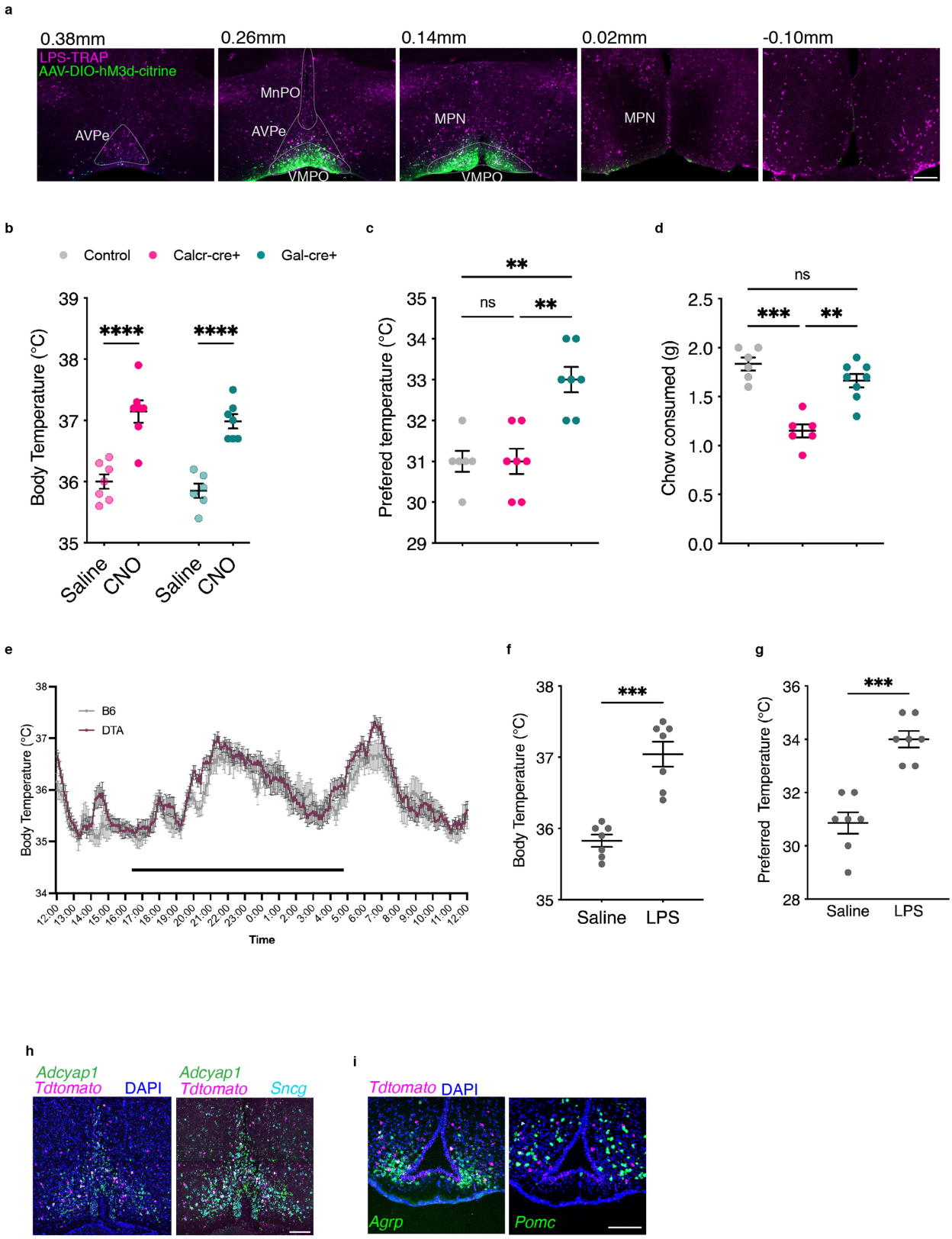

Extended Data Fig. 5 | See next page for caption.

Extended Data Fig. 5 | Specificity of viral injections and cell type identity. (a) Example of viral injection specificity that qualified for inclusion in the study. Note viral expression in the VMPO and absence in surrounding brain areas. Injections found to be more broadly dispersed were not included in analysis. (b-d) Chemogenetic activation of Calcr+ and Gal+ neurons in the VMPO. (b) CNO injection elicited strong increase in body temperature in both genetic backgrounds (n = 6 mice/group). (c) Activation of Gal-Cre but not Calcr-Cre increased preferred temperature (n = 7mice/group). (d) Activation of Calcr-Cre (n = 6 mice) but not Gal-Cre (n = 8) decreased chow consumed (saline n = 6 mice). (e) DTA-mediated Ablation of $VMPO^{LPS}$ neurons had no effect on circadian temperatures, dark bar indicates dark phase, WT mice were used as controls. (f-g) Effect of DTA-mediated ablation of VMPO neurons in Saline-TRAP mice had no effect on body temperature or preferred temperature following LPS injection (n = 7 mice/group). (h) Overlap of warm-TRAP reporter expression with markers of warm-sensitive neurons *adcyap1* and *sncg*. (i) Overlap of hunger-TRAP-mediated reporter expression (magenta) with markers of appetite-increasing neurons, *agrp*, or appetite-decreasing neurons, *pomc*, (green). Scale bars = 200μm. All error bars = SEM. For all graphs * = $p< 0.05$, ** = $p< 0.01$, *** = $p< 0.001$.

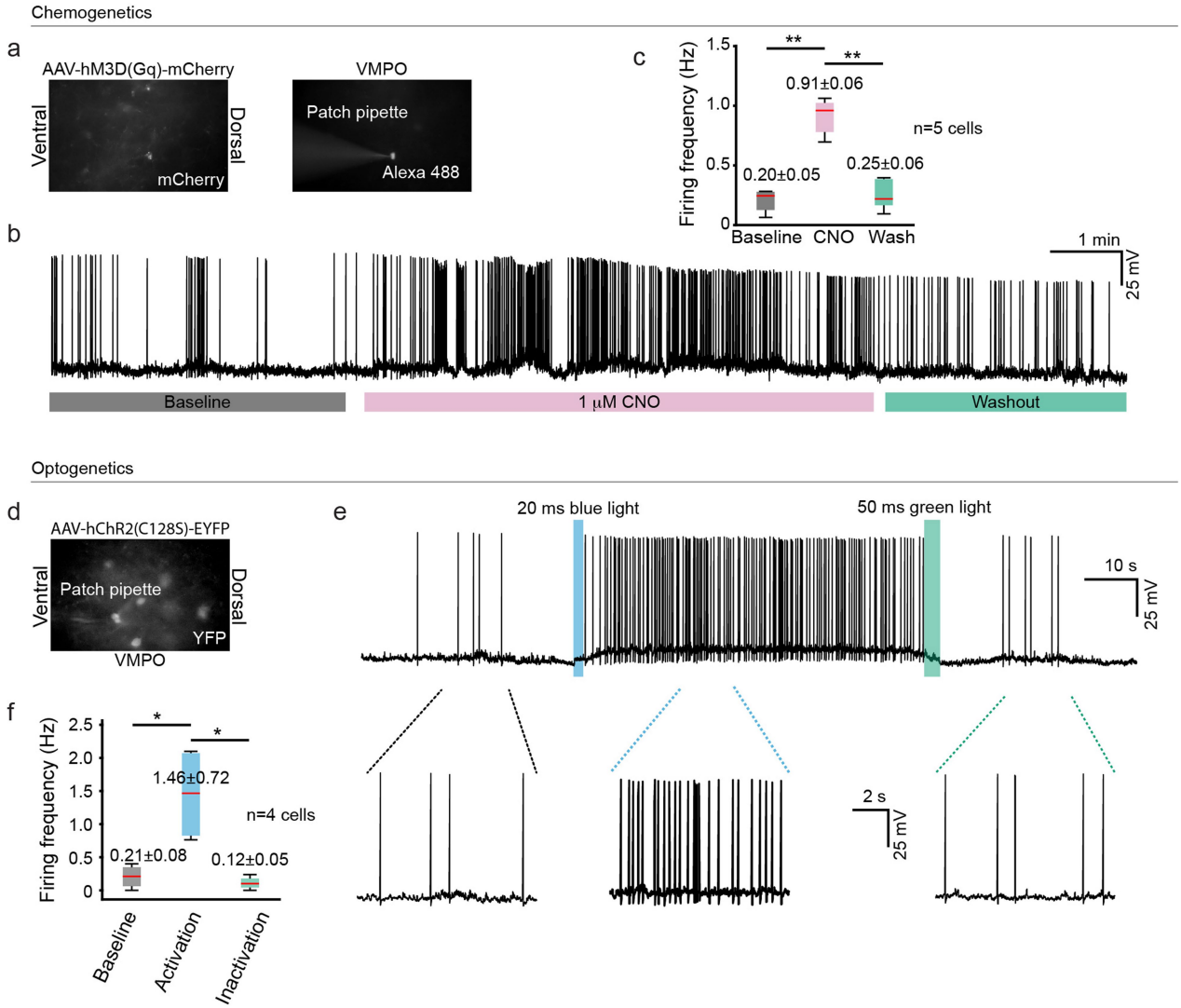

Extended Data Fig. 6 | Chemogenetic and optogenetic activation of VMPO^{LPS} neurons. (a) Widefield microscope images of VMPO^{LPS} neurons in the VMPO of TRAP2 injected with AAV8-hSyn-DIO-hM3D(Gq)-mCherry. (b) Whole cell current clamp recording of a VMPO^{LPS} neuron showing the effects of bath application of 1mM CNO (baseline: black, CNO: pink and washout: green). (c) Effects of CNO application on the firing rate of VMPO^{LPS} neurons; black (n = 5 cells with mean values of 0.20 ± 0.05 Hz for baseline), pink (0.91 ± 0.06 Hz for CNO application and p = 7.0 * 10^{-03} compared to baseline), green (0.25 ± 0.06 Hz for washout and p = 6.9 * 10^{-03} compared to CNO application), boxes represent the 25th and 75th percentile, whiskers extend to the minimum and maximum data points (d) Widefield microscope images of VMPO^{LPS} neurons in the VMPO of TRAP2 injected with AAV5-EF1a-DIO-hChR2(C128S/D156A)-EYFP. (e) Whole cell current clamp recording of a VMPO^{LPS} neuron showing activation of hChR2(C128S/D156A) by 20 ms blue light (460 ± 10 nm) light pulse and inactivation by 50 ms green light (525 ± 9 nm) pulse. (f) Firing rate of VMPO^{LPS} neurons (n = 4 cells) in response to activation of hChR2(C128S/D156A), baseline (black, mean firing frequency of 0.21 ± 0.08 Hz), following blue light activation (blue, mean firing frequency of 1.46 ± 0.72 Hz and p = 2.1 * 10^{-02}) and following green light mediated inactivation of hChR2(C128S/D156A) (green, mean firing frequency of 0.12 ± 0.05 Hz and p = 2.0 * 10^{-02}), boxes represent the 25th and 75th percentile, whiskers extend to the minimum and maximum data points. All p values shown are for two-sided Wilcoxon rank sum test with * = p< 0.05, ** = p< 0, *** = p< 0.005 and ns = p > 0.05.

Extended Data Table 1 | Effects of prostaglandin E2 and cytokines (Il-1β and CCL2) on the intrinsic properties of VMPO^{LPS} neurons

Average values

bath solution	ACSF				IL-1β		IL-1β + Cox2 inhibitor			
		+CCl2	+PGE2	+PGE2 + EP2 Anta.		+PGE2		+PGE2	+PGE2 + EP2 Anta.	
Resting potential	-66.19±0.43	-61.75±0.65	-60.73±0.73	-64.25±0.69	-53.83±0.48	-51.13±0.26	-59.74±0.28	-52.04±0.29	-58.45±0.40	mV
Rheobase current	10.07±0.34	7.10±0.29	6.96±0.30	11.04±0.40	6.67±0.26	5.44±0.25	8.73±0.39	5.73±0.28	9.35±0.24	pA
Peak Ffiring rate	11.09±0.31	10.98±0.48	14.52±0.49	10.92±0.38	18.28±0.37	19.46±0.43	14.27±0.27	19.29±0.39	14.46±0.28	Hz

Comparison accross conditions (p-values, wilcoxon ranksum test)

ACSF	+CCl2		$5.56*10^{-05}$	$9.96*10^{-06}$	$4.52*10^{-02}$	$3.29*10^{-06}$	$2.45*10^{-05}$	$1.20*10^{-05}$	$1.30*10^{-06}$	$1.22*10^{-05}$	+CCl2
			$4.72*10^{-06}$	$1.98*10^{-07}$	$7.61*10^{-02}$	$1.03*10^{-07}$	$2.28*10^{-09}$	$2.89*10^{-02}$	$6.65*10^{-09}$	$2.79*10^{-01}$	
			$7.59*10^{-01}$	$4.01*10^{-05}$	$8.85*10^{-01}$	$3.29*10^{-06}$	$2.45*10^{-05}$	$5.68*10^{-05}$	$1.20*10^{-05}$	$3.21*10^{-05}$	
	+PGE2			$4.55*10^{-01}$		$1.43*10^{-04}$		$1.33*10^{-02}$			
				$7.14*10^{-01}$		$2.91*10^{-01}$		$5.80*10^{-03}$			
				$1.20*10^{-03}$		$1.43*10^{-04}$		$1.51*10^{-04}$			
					$8.90*10^{-03}$	$4.69*10^{-05}$	$1.43*10^{-04}$		$8.73*10^{-05}$	$3.78*10^{-02}$	+PGE2
					$8.94*10^{-08}$	$5.58*10^{-01}$	$2.21*10^{-03}$		$1.18*10^{-02}$	$7.88*10^{-06}$	
					$1.96*10^{-04}$	$6.00*10^{-05}$	$1.43*10^{-04}$		$8.73*10^{-05}$	$7.67*10^{-01}$	
IL-1β							$7.36*10^{-03}$	$8.73*10^{-05}$	$1.01*10^{-02}$	$1.41*10^{-04}$	IL-1β
							$4.20*10^{-03}$	$3.45*10^{-04}$	$2.72*10^{-02}$	$6.05*10^{-07}$	
							$4.97*10^{-02}$	$8.75*10^{-05}$	$1.06*10^{-01}$	$8.75*10^{-05}$	
IL-1β + Cox2 inhibitor									$1.84*10^{-04}$	$3.42*10^{-02}$	IL-1β + Cox2 inhibitor
	+PGE2								$7.28*10^{-06}$	$1.86*10^{-01}$	
									$1.82*10^{-04}$	$6.23*10^{-01}$	
										$1.82*10^{-04}$	+PGE2
										$1.64*10^{-07}$	
										$1.82*10^{-04}$	

Extended Data Table 2 | Effects of prostaglandin E2 and cytokines (Il-1β and CCL2) on the synaptic inputs to VMPO^{LPS} neurons

Average values

bath solution	ACSF				IL-1β		IL-1β + Cox2 inhibitor			
		+CCl2	+PGE2	+PGE2 + EP2 Anta.		+PGE2		+PGE2	+PGE2 + EP2 Anta.	
EPSC amplitude	11.75±0.28	16.30±0.27	12.17±0.53	11.16±0.84	11.76±0.20	11.13±0.25	10.51±0.51	11.58±0.76	11.60±0.41	pA
EPSC inter event interval	54.50±1.20	47.40±1.30	23.60±0.45	57.9±1.10	24.60±1.22	23.90±0.44	52.70±1.31	26.80±0180	58.0±1.5	ms
IPSC amplitude	8.50±0.17	8.21±0.23	6.81±0.24	6.83±0.16	6.71±0.28	6.53±0.25	7.86±0.16	6.64±0.33	6.70±0.21	pA
IPSC inter event interval	55.20±1.10	48.70±1.02	85.70±5.30	85.4±6.80	86.40±4.20	88.20±3.50	54.60±2.70	87.40±2.90	84.70±3.60	ms

Comparison accross conditions (p-values, wilcoxon ranksum test)

		ACSF	+CCl2	+PGE2	+PGE2 + EP2 Anta.	IL-1β	+PGE2	IL-1β + Cox2 inhibitor	+PGE2	+PGE2 + EP2 Anta.	
ACSF	+CCl2			$7.12*10^{-05}$	0.7920	0.9336	0.9809	0.6368	0.592	0.6769	0.9759
				$1.40*10^{-03}$	$1.77*10^{-05}$	0.3047	$1.87*10^{-05}$	$7.2*10^{-05}$	0.5490	$7.13*10^{-05}$	0.1238
				0.2547	$7.63*10^{-05}$	$1.12*10^{-04}$	$2.45*10^{-04}$	$5.38*10^{-05}$	$3.07*10^{-02}$	$1.45*10^{-04}$	$1.91*10^{-04}$
				$2.01*10^{-03}$	$1.78*10^{-05}$	$1.13*10^{-04}$	$1.77*10^{-05}$	$7.12*10^{-05}$	0.9846	$7.26*10^{-05}$	$1.55*10^{-04}$
	+PGE2		$9.14*10^{-05}$			$4.57*10^{-05}$		$4.23*10^{-05}$			
			$4.50*10^{-05}$			$4.56*10^{-05}$		$1.17*10^{-02}$			
			$3.19*10^{-04}$			$4.41*10^{-03}$		0.4235			
			$3.59*10^{-05}$			$5.47*10^{-05}$		0.1228			
	+PGE2			0.6334	0.6232	0.2370	0.0539	0.6334	0.6009		
				$4.57*10^{-05}$	0.9097	0.4082	$1.82*10^{-04}$	0.1728	$1.02*10^{-04}$		
				0.8968	0.7337	0.3883	$4.10*10^{-03}$	0.7618	0.8286		
				0.9654	0.8501	0.7618	$3.29*10^{-04}$	0.6965	0.9623		
IL-1β						0.1457	0.0640	0.9654	0.8125		
						0.8782	$1.83*10^{-04}$	0.3154	$1.28*10^{-04}$		
						0.6602	$7.6*10^{-03}$	0.8463	0.8165		
						0.4018	$1.83*10^{-04}$	0.5148	0.9685		
IL-1β + Cox2 inhibitor	+PGE2							0.3599	0.1932		
								$2.51*10^{-03}$	$1.62*10^{-02}$		
								$4.57*10^{-05}$	$2.51*10^{-02}$		
								$4.12*10^{-05}$	$1.02*10^{-04}$		
									0.7789		
									$3.11*10^{-04}$		
									0.9591		
									0.6126		

Extended Data Table 3 | Abbreviations of brain areas

ACB	nucleus accumbens
Arc	arcuate nucleus
BLA	basolateral amygdala
BNST	bed nucleus of the stria terminalis
CEA	central amygdala
DMH	dorsal medial hypothalamus
IC	insular cortex
LC	locus coeruleus
LH	lateral hypothalamus
LPB	lateral parabrachial nucleus
LS	lateral septum
NTS	nucleus tractus solitarius
PAG	periaqueductal gray
PBNc	parabrachial nucleus complex
PMD	dorsal premammillary nucleus
PMV	ventral premammillary nucleus
PSTh	parasubthalamic nucleus
PVH	paraventricular nucleus of the hypothalamus
PVT	paraventricular nucleus of the thalamus
StHy	striohypothalamic nucleus
TU	tuberal nucleus
vBNST	ventral part of the BNST
VLPO	ventral lateral preoptic area
VMPO	ventral medial preoptic area

Abbreviations of brain areas

Extended Data Table 4 | List of drugs

Drug name	Company name	Solvent	Stock conc.	Working Conc.
CNQX disodium salt	Hello Bio	Water	20 mM	20 μM
D-AP5	Hello Bio	Water	50 mM	50 μM
Gabazine	Hello Bio	Water	20 mM	20 μM
TTX citrate	Hello Bio	Water	1 mM	1 μM
QX-314 bromide	Tocris	Recording solution	50 mM	5 mM
Prostaglandin E2	Tocris	Ethanol	20 mM	1 μM
Mouse CCL2	R&D systems	ACSF	250 nM	2.5 nM
IL-1β	R&D systems	ACSF	50 nM	1 nM
NS-398 (COX-2 inhibitor)	Cayman chemicals	DMSO	80 mM	20 μM
PF 04418948 (EP2 antagonist)	Cayman chemicals	DMSO	50 mM	10 μM
Clozapine N-oxide	Sigma Aldrich	DMSO	10 mM	1-10 μM

Extended Data Table 5 | Precise animal numbers for Fig. 3

Figure 3 Panel:	C	F	M	N	O	P	Q	R
AAV-GFP, Cre+	13	9	10	10	10	10	11	8
AAV-hM3D/DTA, Cre-	12	13	12	10	14	10	9	7
AAV-hM3D/DTA, Cre+	12	9	14	8	8	9	9	7

Extended Data Table 6 | Precise cell numbers for Fig. 2 and Extended Data Fig. 4

Figure panels:	Fig. 2g-h, Ext. Data Fig. 4b	Ext. Data Fig. 4d-e, Ext Data Fig. 4h-i	Fig. 2i-j, Ext. Data Fig. 4c	Ext. Data Fig. 4f-g Ext. Data Fig. 4j-k	Fig. 2L	Ext. Data Fig. 4m
Control	20	18	20	18	18	10
CCL2	9	8			8	8
PGE2	12	10			10	
PGE2 + EP2 antagonist	11	8				
IL-1β	12	10	12	10	10	
IL-1β + PGE2	9	8				
IL-1β + COX2 inhibitor			10	10		
IL-1β + COX2 inhibitor +PGE2			10	8		
IL-1β + COX2 inhibitor +PGE2 +EP2 antagonist			10	7		

nature research

Corresponding author(s): Catherine Dulac

Last updated by author(s): Feb 26, 2022

Reporting Summary

Nature Research wishes to improve the reproducibility of the work that we publish. This form provides structure for consistency and transparency in reporting. For further information on Nature Research policies, see Authors & Referees and the Editorial Policy Checklist.

Statistics

For all statistical analyses, confirm that the following items are present in the figure legend, table legend, main text, or Methods section.

n/a	Confirmed	
☐	☒	The exact sample size (*n*) for each experimental group/condition, given as a discrete number and unit of measurement
☐	☒	A statement on whether measurements were taken from distinct samples or whether the same sample was measured repeatedly
☐	☒	The statistical test(s) used AND whether they are one- or two-sided *Only common tests should be described solely by name; describe more complex techniques in the Methods section.*
☐	☒	A description of all covariates tested
☐	☒	A description of any assumptions or corrections, such as tests of normality and adjustment for multiple comparisons
☐	☒	A full description of the statistical parameters including central tendency (e.g. means) or other basic estimates (e.g. regression coefficient) AND variation (e.g. standard deviation) or associated estimates of uncertainty (e.g. confidence intervals)
☐	☒	For null hypothesis testing, the test statistic (e.g. *F*, *t*, *r*) with confidence intervals, effect sizes, degrees of freedom and *P* value noted *Give P values as exact values whenever suitable.*
☒	☐	For Bayesian analysis, information on the choice of priors and Markov chain Monte Carlo settings
☒	☐	For hierarchical and complex designs, identification of the appropriate level for tests and full reporting of outcomes
☒	☐	Estimates of effect sizes (e.g. Cohen's *d*, Pearson's *r*), indicating how they were calculated

Our web collection on statistics for biologists contains articles on many of the points above.

Software and code

Policy information about availability of computer code

Data collection	Fluorescent images were collected using Zen Blue (v3.4) and Axiovision r software (v4.8) from Zeiss. Temperature preference data was collected using the Thermal Gradient Test software from Bioseb. Locomotion was tested using Ethovision XT 8.0 from Noldus Information Technology. RNAscope in situ data was analyzed using Cell Profiler (v2.2) from the Broad Institute. Custom Matlab code was used to quantify cfos+ cells, which will be made available upon request. MERFISH image analysis was performed using code freely available at github. com/ Zhuanglab/MERlin. Electrophysiological data were collected via software written in LabView (National Instruments) and pClamp 10.3 (Molecular Devices). A custom written software (MATLAB) was used to measure the timing of action potentials and the firing rates of neurons. The template match algorithm in Axograph (1.7.6) was used to measure the amplitude, timing, and inter-event intervals of synaptic events.
Data analysis	Statistical analyses were performed in Graphpad Prism 8.0c or using standard Matlab or R routines.

For manuscripts utilizing custom algorithms or software that are central to the research but not yet described in published literature, software must be made available to editors/reviewers. We strongly encourage code deposition in a community repository (e.g. GitHub). See the Nature Research guidelines for submitting code & software for further information.

Data

Policy information about availability of data

All manuscripts must include a data availability statement. This statement should provide the following information, where applicable:

- Accession codes, unique identifiers, or web links for publicly available datasets
- A list of figures that have associated raw data
- A description of any restrictions on data availability

Sequencing data that support the findings of this study have been deposited in Gene Expression Omnibus under accession number GSE197547. All other data that support the findings of this study are either present in figures and extended data or available from the corresponding author upon reasonable request.

Field-specific reporting

Please select the one below that is the best fit for your research. If you are not sure, read the appropriate sections before making your selection.

☒ Life sciences ☐ Behavioural & social sciences ☐ Ecological, evolutionary & environmental sciences

For a reference copy of the document with all sections, see nature.com/documents/nr-reporting-summary-flat.pdf

Life sciences study design

All studies must disclose on these points even when the disclosure is negative.

Sample size	No statistical methods were used to predetermine sample size, but sample sizes are consistent with those generally employed in the field (Wu et al 2014, Tan et al 2016, Takahashi et al 2020)
Data exclusions	In chemogenetic and ablation experiments, mice with no expression of the virus or virus injections outside the vicinity of the VMPO were excluded from the analysis. Mice that did not have a fever during LPS-TRAP procedure were excluded from further experiments.
Replication	Behavior and neuronal activity manipulation experiments were replicated independently >3 times. Expression data was replicated independently at least twice. All attempts at replication were successful.
Randomization	Animals were randomly assigned numbers for the experimental condition.
Blinding	Behavior was scored automatically by computer programs and not subject to interpretation by individuals. Parameters for automatic behavior quantification, including calibrations were unchanged between groups. Quantification of cell numbers and marker overlap was blinded to the investigator. Analysis of tracing experiments was non blinded to the investigator. Analysis of electrophysiological data was automated by computer programs and not subject to interpretation by the investigator.

Reporting for specific materials, systems and methods

We require information from authors about some types of materials, experimental systems and methods used in many studies. Here, indicate whether each material, system or method listed is relevant to your study. If you are not sure if a list item applies to your research, read the appropriate section before selecting a response.

Materials & experimental systems

n/a	Involved in the study
☐	☒ Antibodies
☒	☐ Eukaryotic cell lines
☒	☐ Palaeontology
☐	☒ Animals and other organisms
☒	☐ Human research participants
☒	☐ Clinical data

Methods

n/a	Involved in the study
☒	☐ ChIP-seq
☒	☐ Flow cytometry
☒	☐ MRI-based neuroimaging

Antibodies

Antibodies used	Primary antibodies: Rabbit anti-c-Fos (9F6; Cell Signaling), 1:1000. Chicken anti-GFP (ab13970, Abcam), 1:1000. Secondary antibodies (all from Life tehcnologies): Alexa-488 anti-rabbit (A21206) 1:1000, Alexa-568 anti-rabbit (A11011) 1:1000, and Alexa-647 anti-rabbit (A21245) 1:1000, Alexa-488 anti-chicken (A32931) 1:1000.
Validation	Rabbit anti-c-Fos was validated using alternative c-Fos antibodies in tissue with known expression patterns. In addition, the manufacturers report that this antibody is specific to human, mouse and rat c-Fos protein and was validated by the manufacturers using western blot and for ChIP analysis: "This antibody has been validated using SimpleChIP Enzymatic Chromatin IP kits". Chicken anti-GFP antibody was validated using endogenous GFP expression in tissue sections as well as by the manufacturer using western blot, immunohistochemistry and immunofluorescence. According to the manufacturer, this GFP antibody does cross-react with the many fluorescent proteins that are derived from the jellyfish Aequorea victoria. These are all proteins that differ from the original GFP by just a few point mutations (EGFP, YFP, mVenus, CFP, BFP etc.)

Animals and other organisms

Policy information about studies involving animals; ARRIVE guidelines recommended for reporting animal research

Laboratory animals	The following mouse strains were used at 8-24 weeks depending on experiment, as detailed in the methods section: C57BL/6J, TRAP2 (Fos2A-iCreER), Ai9(RCL-tdT), Calcr-Cre, Gal-Cre. Only male mice were used for experiments.

Wild animals	This study did not involve wild animals
Field-collected samples	This study did not involve field samples
Ethics oversight	All experiments were performed in accordance with NIH guidelines and approved by the Harvard University Institutional Animal Care and Use Committee (IACUC).

Note that full information on the approval of the study protocol must also be provided in the manuscript.